AD-A196 574

DTIC FILE COPY

A Final Report
Grant No. N00014-87-K-0042
December 1, 1986 - July 31, 1988

THE INFLUENCE OF CATHODIC PROTECTION ON EROSION-CORROSION OF METALS AND MODEL ALLOYS

Submitted to:

Office of Naval Research
800 N. Quincy Street
Arlington, VA 22217-5000

Attention: Dr. A. John Sedriks
Materials Division, Code 1131M

Submitted by:

Mark E. Orazem
Assistant Professor

Report No. UVA/525418/CHE88/102
June 1988

DTIC ELECTE JUN 28 1988 S D

This document has been approved for public release and sale; its distribution is unlimited.

SCHOOL OF ENGINEERING AND APPLIED SCIENCE

DEPARTMENT OF CHEMICAL ENGINEERING

UNIVERSITY OF VIRGINIA
CHARLOTTESVILLE, VIRGINIA 22901

88 6 33

A Final Report
Grant No. N00014-87-K-0042
December 1, 1986 - July 31, 1988

THE INFLUENCE OF CATHODIC PROTECTION ON EROSION-CORROSION OF METALS AND MODEL ALLOYS

Submitted to:

Office of Naval Research
800 N. Quincy Street
Arlington, VA 22217-5000

Attention: Dr. A. John Sedriks
Materials Division, Code 1131M

Submitted by:

Mark E. Orazem
Assistant Professor

Department of Chemical Engineering
SCHOOL OF ENGINEERING AND APPLIED SCIENCE
UNIVERSITY OF VIRGINIA
CHARLOTTESVILLE, VIRGINIA

Accession For
NTIS GRA&I [X]
DTIC TAB [ ]
Unannounced [ ]
Justification
By
Distribution/
Availability Codes
Dist | Avail and/or Special
A-1

Report No. UVA/525418/CHE88/102
June 1988

Copy No.

DTIC

This document has been approved for public release and sale; its distribution is unlimited.

REPORT DOCUMENTATION PAGE

1a. REPORT SECURITY CLASSIFICATION Unclassified	1b. RESTRICTIVE MARKINGS None
2a. SECURITY CLASSIFICATION AUTHORITY	3. DISTRIBUTION / AVAILABILITY OF REPORT Approved for public release; distribution unlimited
2b. DECLASSIFICATION / DOWNGRADING SCHEDULE	
4. PERFORMING ORGANIZATION REPORT NUMBER(S) UVA/525418/CHE88/102	5. MONITORING ORGANIZATION REPORT NUMBER(S)
6a. NAME OF PERFORMING ORGANIZATION Dept. of Chemical Engineering University of Virginia 6b. OFFICE SYMBOL (*If applicable*)	7a. NAME OF MONITORING ORGANIZATION Office of Naval Research Resident Representative
6c. ADDRESS (*City, State, and ZIP Code*) Thornton Hall Charlottesville, VA 22901	7b. ADDRESS (*City, State, and ZIP Code*) 818 Connecticut Avenue, NW, Eighth Floor Washington, DC 20006
8a. NAME OF FUNDING / SPONSORING ORGANIZATION Office of Naval Research 8b. OFFICE SYMBOL (*If applicable*)	9. PROCUREMENT INSTRUMENT IDENTIFICATION NUMBER N00014-87-K-0042
8c. ADDRESS (*City, State, and ZIP Code*) 800 N. Quincy Street Arlington, VA 22217-5000	10. SOURCE OF FUNDING NUMBERS PROGRAM ELEMENT NO. / PROJECT NO. / TASK NO. / WORK UNIT ACCESSION NO.

11. TITLE (*Include Security Classification*)
The Influence of Cathodic Protection on Erosion-Corrosion of Metals and Model Alloys

12. PERSONAL AUTHOR(S)
M. E. Orazem

13a. TYPE OF REPORT	13b. TIME COVERED	14. DATE OF REPORT (*Year, Month, Day*)	15. PAGE COUNT
Final	FROM 12/31/86 TO 07/31/88	1988 June 14	26

16. SUPPLEMENTARY NOTATION

17. COSATI CODES			18. SUBJECT TERMS (*Continue on reverse if necessary and identify by block number*)
FIELD	GROUP	SUB-GROUP	

19. ABSTRACT (*Continue on reverse if necessary and identify by block number*)

The object of this program is to develop a fundamental understanding of the influence of applied potential on mechanisms for erosion-corrosion as applied to copper and copper-based alloys. This work is intended to allow application of laboratory experiments to predict the onset of erosion-corrosion failure under field conditions and to guide development of workable strategies for prevention of erosion-corrosion. This program is being transferred to the University of Florida; therefore, this report provides a summary of the activities at the University of Virginia.

20. DISTRIBUTION / AVAILABILITY OF ABSTRACT ☒ UNCLASSIFIED/UNLIMITED ☐ SAME AS RPT ☐ DTIC USERS	21. ABSTRACT SECURITY CLASSIFICATION Unclassified
22a NAME OF RESPONSIBLE INDIVIDUAL Dr. A. John Sedriks	22b. TELEPHONE (*Include Area Code*) / 22c. OFFICE SYMBOL

DD FORM 1473, 84 MAR — 83 APR edition may be used until exhausted. All other editions are obsolete

SECURITY CLASSIFICATION OF THIS PAGE
Unclassified

19. *In the first year of the program, an electrochemical cell incorporating a scanning ellipsometer was designed and built. The cell uses a submerged electrolyte jet impinging on an electrode. The laser spot size is around 25 × 70 μm, and the position of the electrode–jet assembly relative to the laser spot can be controlled by stepping motor stages without altering the hydrodynamic environment. This system will be used to map local film thickness under well controlled fluid flow exhibiting high shear rates. The radial position at which the film thickness decreases can be related to a critical value for hydrodynamic shear required to remove the film, and the use of a well–characterized flow geometry allows separation of erosion–corrosion effects from corrosion enhancement associated with mass transfer. Experiments using this system will begin in the second year of the program. In support of the erosion–corrosion studies, electrochemical experiments are being conducted to identify the corrosion mechanisms and film composition associated with corrosion of copper in neutral and basic saline solutions. These experiments will be extended to model copper–aluminum alloys in the second year of the program.*

Abstract

The object of this program is to develop a fundamental understanding of the influence of applied potential on mechanisms for erosion–corrosion as applied to copper and copper–based alloys. This work is intended to allow application of laboratory experiments to predict the onset of erosion–corrosion failure under field conditions and to guide development of workable strategies for prevention of erosion–corrosion. This program is being transferred to the University of Florida; therefore, this report provides a summary of the activities at the University of Virginia.

In the first year of the program, an electrochemical cell incorporating a scanning ellipsometer was designed and built. The cell uses a submerged electrolyte jet impinging on an electrode. The laser spot size is around 25 × 70 μm, and the position of the electrode–jet assembly relative to the laser spot can be controlled by stepping motor stages without altering the hydrodynamic environment. This system will be used to map local film thickness under well controlled fluid flow exhibiting high shear rates. The radial position at which the film thickness decreases can be related to a critical value for hydrodynamic shear required to remove the film, and the use of a well–characterized flow geometry allows separation of erosion–corrosion effects from corrosion enhancement associated with mass transfer. Experiments using this system will begin in the second year of the program. In support of the erosion–corrosion studies, electrochemical experiments are being conducted to identify the corrosion mechanisms and film composition associated with corrosion of copper in neutral and basic saline solutions. These experiments will be extended to model copper–aluminum alloys in the second year of the program.

Scientific Research Goals

Erosion–corrosion is a pervasive and complex problem which is attributed to velocity–enhanced mass transfer as well as to a mechanical removal of protective oxide films. The objective of this contract, awarded January 20, 1987, is to identify specific modes of corrosion enhancement associated with high–speed flow. This work is necessary to provide a fundamental understanding of the mechanism for erosion–corrosion, and to allow application of laboratory experiments to field conditions. This work is intended to guide development of workable strategies for prevention of erosion–corrosion.

This objective will be accomplished by developing a new experimental system to study the erosion–corrosion of copper and model copper–based alloys in sodium chloride solutions. The growth and removal of oxide films will be observed *in–situ* by automated scanning ellipsometry. This apparatus will be used to study the electrochemistry of copper and model copper–based alloys under conditions where erosion–corrosion is expected. These materials were chosen because they are of industrial and national importance and because

they are known to be susceptible to erosion–corrosion attack. Parametric studies will be conducted to identify the mode of enhanced attack, the influence of fluid composition and pH, and the influence of polarization. The ultimate goal of this work is the development of a mathematical model to predict the current requirements for the cathodic protection of complex geometries subject to high–speed flow. In order to provide a comprehensive solution to the problem, local microstructural and microchemical analyses will also be employed. The techniques to be used include scanning and transmission electron microscopy, energy dispersive X–ray analysis, and Auger spectroscopy.

Significant Results

The results of the first year include design and construction of an ellipsometer to measure local film thickness under high–speed impinging fluid, preliminary electrochemical experiments for copper in neutral and basic saline solutions, and development of an in–house capability to formulate model copper–aluminum alloys. The experimental design used here has been presented at *Corrosion/88.** Two papers, supported in part by this contract, are presented in *Appendix A*. The first paper† covers development of a computer program used to compensate for ohmic resistance and to identify the current distribution on a disk electrode. Use of this program will allow us to identify conditions where the current distribution should be uniform, essential when using current distribution to characetrize the effects of high–shear flow (see the discussion of Figure 4). The second paper‡ provides guidelines for the use of recessed electrodes to eliminate the complications associated with the nonuniform current and potential distributions seen on flush–mounted disk electrodes. This may be used to eliminate errors during electrochemical A. C. impedance spectroscopy of the copper alloys.

---

* C. B. Diem and M. E. Orazem, "A Scanning Ellipsometer to Evaluate the Influence of Fluid Velocity on Corrosion," presented at the T–5A Workshop on Fluid Flow Enhanced Corrosion, Corrosion/88, Saint Louis, Missouri, March 23, 1988.

† J. M. Esteban, M. Lowry, and M. E. Orazem, "Correction of Experimental Data for the Ohmic Potential Drop Corresponding to a Secondary Current Distribution on a Disk Electrode," (invited paper) presented at the ASTM Symposium on Ohmic Electrolyte Resistance Measurement and Compensation, Baltimore, Maryland, May 19, 1988. Also submitted for the *ASTM Special Technical Publication on Ohmic Electrolyte Resistance Measurement and Compensation.*

‡ C. B. Diem, B. Newman, and M. E. Orazem, "The Influence of Small Machining Errors on the Primary Current Distribution at a Recessed Electrode," *Journal of the Electrochemical Society*, in press.

Cell Design

Our primary goal for the first year was to design and construct the impinging jet/ellipsometer apparatus. The cell has been designed and constructed. A schematic representation of the cell is shown in Figure 1. This includes computer–interfaced stepping motor stages for accurate positioning of the jet nozzle and metal electrode to be studied, polarizer and analyzer components of the ellipsometer, and a plexiglas cell compartment supported in a rigid 1/2 inch aluminum frame. The flow assembly is given as Figure 2. A magnetically coupled centrifugal pump will be used to drive the flow, and the system is designed to allow study of both aerated and deaerated conditions. The flow system has been tested, and the ellipsometer has been installed and is being calibrated. This system will be controlled by a HP 310 laboratory computer, and most of the software needed to run these experiments has been written. The underlying concept and principles for the cell design are presented in the following sections.

Concept

In the absence of impingement of particles or bubbles, hydrodynamic shear is the primary mechanism for transfer of momentum between the flowing electrolyte and the surface (see references 1-3). A nonzero value for the wall shear stress results from the relative motion between the fluid and the solid. This force acts on the surface in the direction of flow, and has been implicated in the removal of loosely adherent films. Copson[4] suggested that shear stresses are likely to be too small to cause significant erosion–corrosion. Indeed, experiments conducted in our laboratory indicate that if particles or small bubbles are present in the flowing electrolyte, attack by impingement will overwhelm attack by shear mechanisms. Efird[5] has reported critical values of shear stress for the erosion–corrosion of copper and some copper–based alloys in sea water. The temperature dependence of the critical velocity was shown to correlate well with the temperature dependence of the surface shear stress. Giralt and Trass[6] have shown that removal of solid naphthalene and trans–cinnamic acid by a submerged impinging jet of saturated solution is proportional to the wall shear stress above a critical or threshold value. Steele and Geankoplis[7] have also reported removal of material by an apparent shear erosion mechanism.

The concept of a critical shear stress may allow a more universal application of erosion–corrosion experiments. It is well known that values obtained for critical velocities in different experimental systems do not agree. Since, in the absence of mass transfer or impingement effects, the means of transfer of momentum from the fluid to the solid is the shear stress, the extent of erosion–corrosion by shear would be expected to be the same for different geometries only if the value of shear stress would be the same. This approach has been suggested by Efird[5] and by Silverman.[8] The use of this approach requires that experiments be conducted for which the effects of mass transfer, impingement, and shear can be quantitatively assessed.

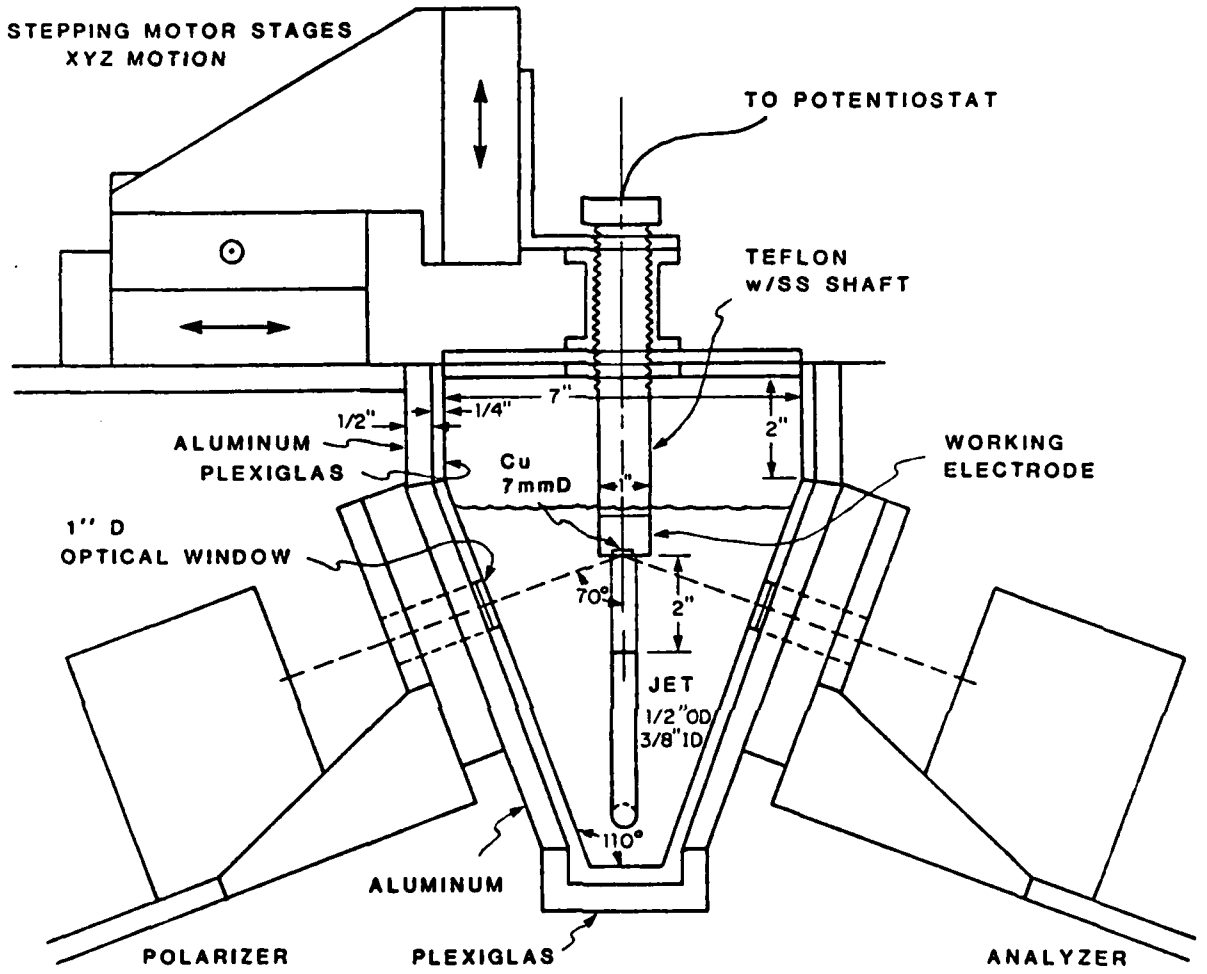

Figure 1. Schematic representation of the cell used in the impinging-jet apparatus for *in-situ* study of the erosion-corrosion of copper and copper-based alloys.

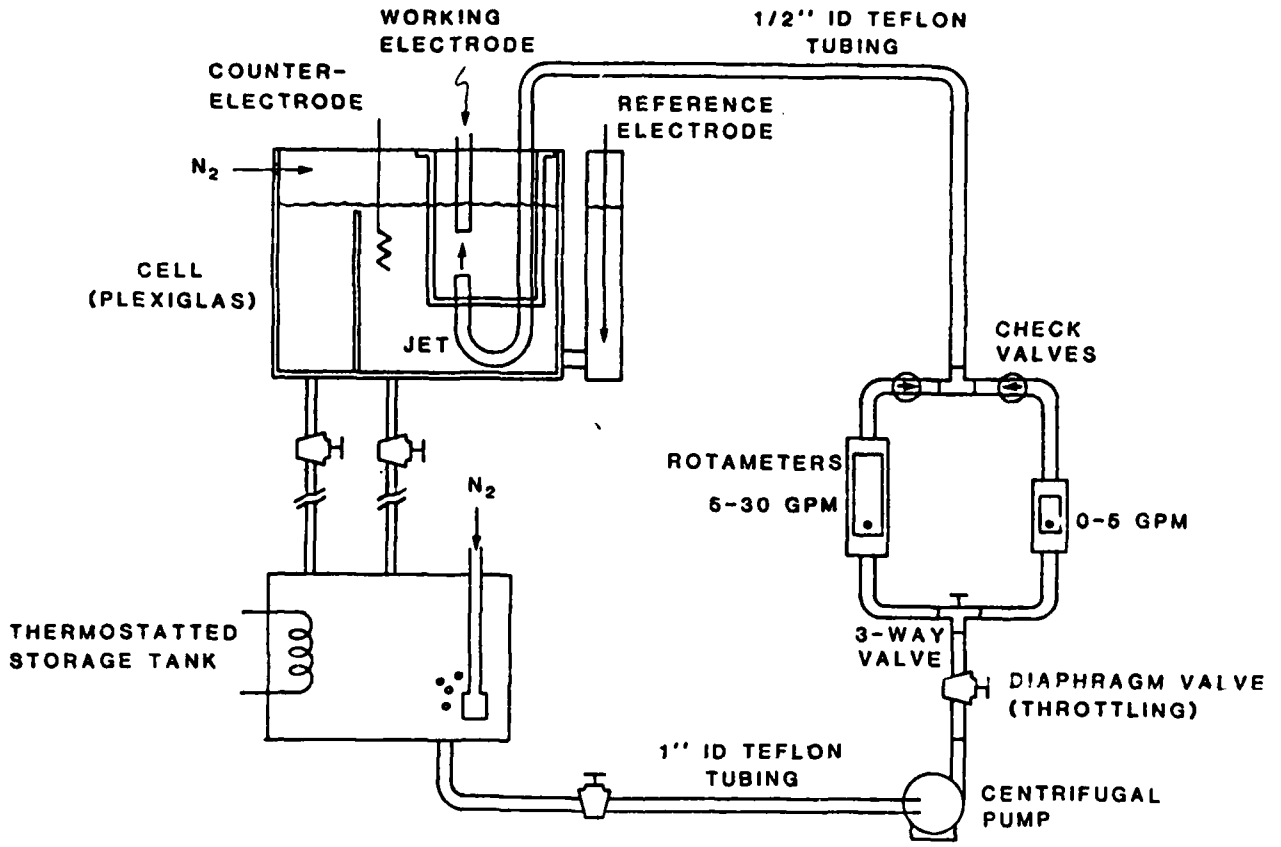

Figure 2. Schematic representation of the flow–system design for the impinging–jet apparatus for *in–situ* study of the erosion–corrosion of copper and copper–based alloys.

The Impinging Jet Electrode

The impinging jet system comprises a submerged electrolyte jet impinging at 90° onto a flat specimen. The flow pattern for this system has been studied extensively[9-16] and is shown in Figure 3. Detailed mathematical analyses for this system have tended to concentrate on the stagnation and wall jet regions. The stagnation region is observed directly beneath the jet. Within the stagnation region, the axial velocity is independent of radial position. The flow in this region therefore resembles a rotating disk in that the surface is uniformly accessible to mass transfer. Further from the center line, a boundary layer is developed which is called the wall jet region.

The velocity distribution in the stagnation region has both radial and axial components. The velocity in the radial direction is given by[16]

$$v_r = ar\frac{df(\eta)}{d\eta}, \tag{1}$$

and the velocity in the axial direction is given by

$$v_z = -2\sqrt{a\mu/\rho}\, f(\eta); \tag{2}$$

where

$$f(\eta) = 0.656\eta^2 - \frac{1}{6}\eta^3 + 3.6444 \times 10^3\eta^6 + O(\eta^7),$$

and $\eta = \sqrt{a\rho/\mu}\, z$. The parameter a in equations (1) and (2) is the hydrodynamic constant with units of s^{-1}. It plays a role in the impinging jet system similar to that of rotation speed in a rotating disk system. The hydrodynamic constant is a function of jet velocity and the distance between the nozzle and the electrode and can be determined through independent electrochemical experiments. The fluid viscosity μ and density ρ are also measured independently.

The axial velocity is independent of radial position. Thus, a mass-transfer-limited current distribution across the electrode is uniform. The radial velocity is a function of radial position; it has a value of zero at the center of the disk and has a maximum value at the outer edge of the disk. Both the radial and axial velocities obey the no-slip boundary condition and are zero at the wall. The only non-zero value of surface shear stress is τ_{rz}, given by

$$\tau_{rz} = -1.312r(\mu\rho)^{1/2}a^{3/2}. \tag{3}$$

The shear stress is a linear function of radial position. It has a value of zero at the center of the disk and reaches a maximum value at the outer edge of the disk. The parameter a is the hydrodynamic constant which is proportional to the average jet velocity. The flow in the wall jet region is more complex and is described by Scholtz and Trass.[13]

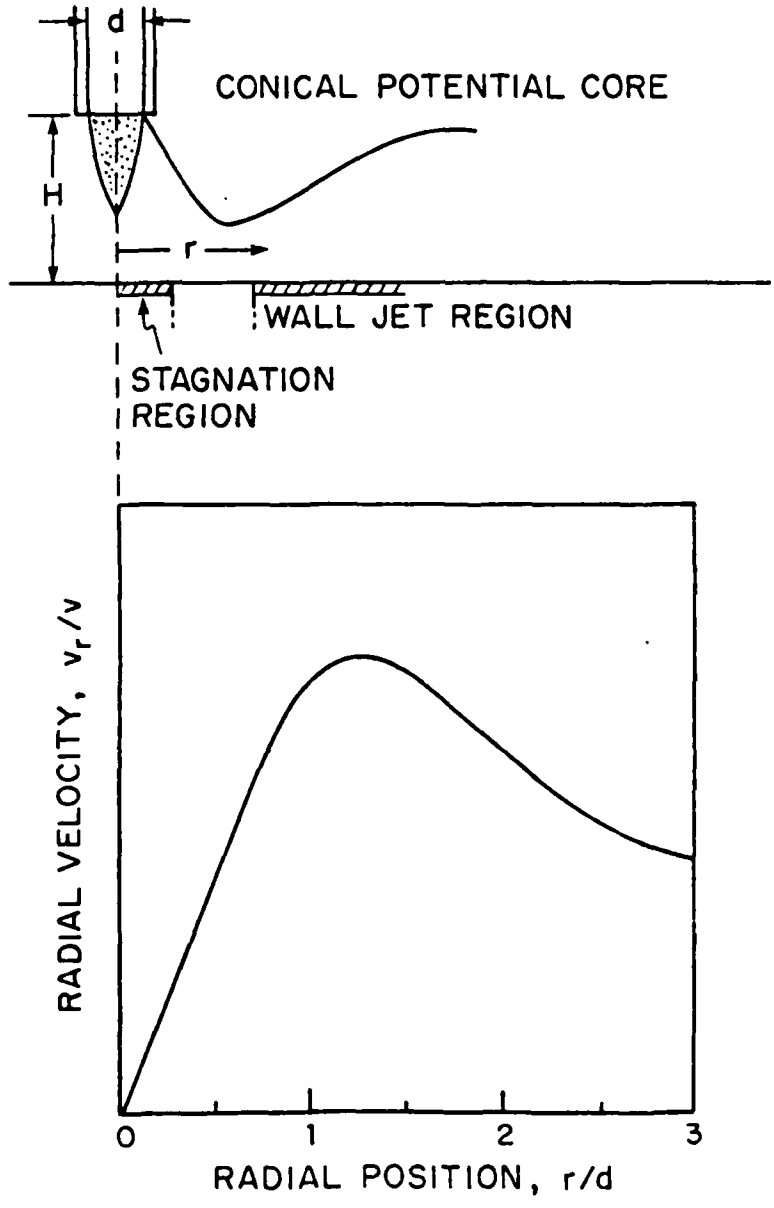

Figure 3. The flow pattern for a submerged impinging jet.

Experimental Method

Two aspects of experimental method are discussed here. The primary pbjective of this work is the measurement of the persistency of oxide films under high–shear flow. A second important aspect is the determination of the hydrodynamic constant a, which plays a role for the impinging jet that is similar to that of the rotation speed of a rotating disk electrode. The hydrodynamic constant, however, must be measured through independent experiments.

Measurement of Film Persistency. The impinging–jet system provides a unique environment for the electrochemical evaluation of film persistency. It can be used to distinguish clearly among the various modes of erosion–corrosion. The approach taken to identify a shear mode for removal of a film is illustrated in Figure 4. The shear stress on the electrode surface for a given average jet velocity is a linear function of radial position. The critical shear (τ_c) for removal of a protective film can, in principle, be obtained by measuring the profile of an electrode subjected to a given jet velocity. For velocity v_1, the radial position at which a sudden increase in corrosion rates is observed (r_{c1}) provides a value for the critical shear. The rate of corrosion at larger values of radial position can be determined from the electrode profiles, and these values provide the proportionality of erosion–corrosion rate to shear stress. At the higher jet velocity (v_2), the critical shear should be observed at a smaller radial position (r_{c2}). Thus, a single experiment can be used to scan a continuous distribution of wall shear stress values and thereby obtain the critical value. Experiments conducted at different velocities provide verification for the critical shear values.

Calculations similar to those presented by Newman[17] can be used to determine whether a nonuniform current distribution is expected from mass–transfer and potential distribution considerations. A numerical method for determining the current distribution from experimental current–potential data in the Tafel regime has been developed in this laboratory (see *Appendix A: Papers Supported by this Contract.*[18–20] Usually, if a surface is protected by a film, the current distribution predicted by these calculations will be uniform. Therefore, if the corrosion is mass–transfer controlled, the enhanced corrosion rates will be uniform and not exhibit a critical radius. The use of profilometry provides information that is otherwise submerged in a simple weight–loss measurement, and these measurements provide an indirect proof of a shear mechanism for erosion-corrosion. This has been used here in the study of the persistency of inhibitor films;[21–23] however, this work also showed the need for a direct measure of film persistency. Direct proof may be obtained by the use of scanning ellipsometry to measure local film thicknesses which should change in the presence of erosion–corrosion.

The advantages of this technique are:

- The fluid flow is well characterized. The hydrodynamic shear for the impinging-jet system in the stagnation region is a linear function of radial position and can be measured through a sensitive electrochemical technique.
- Mass transfer to the disk is uniform. This prevents establishment of differential oxygenation cells and aids in the interpretation of experimental results. Fortunately, the constraint on electrode size given by the need for uniform mass transfer does not significantly reduce the maximum values of wall shear stress that can be reached as compared

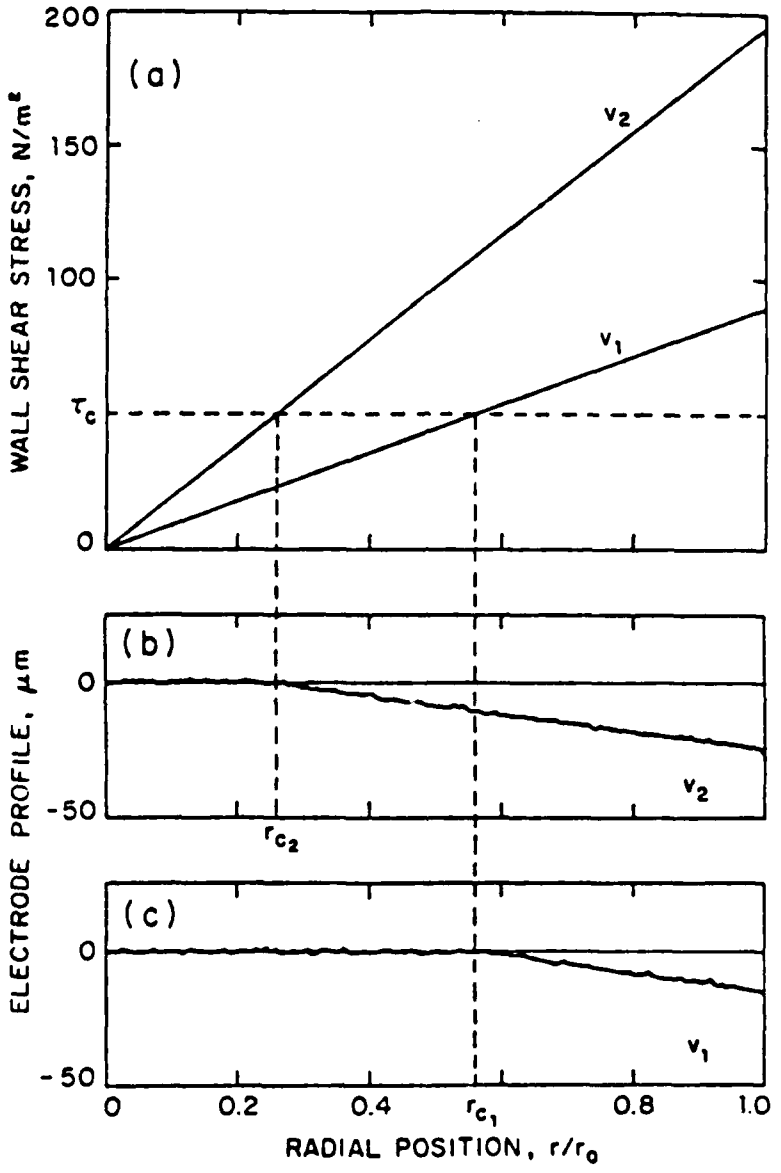

Figure 4. The use of electrode profile (or measured film thickness distribution) to identify a critical wall shear stress for removal of a protective film: a) wall shear stress as a function of radial position with jet velocity as a parameter; b) electrode profile as a function of radial position after sustained corrosion under jet velocity v_2; and c) electrode profile as a function of radial position after sustained corrosion under jet velocity v_1.

to the current practice. The wall shear stress reaches a maximum close to the radius where the mass transfer is no longer uniform.

- The electrode is stationary. This allows use of *in-situ* determination of film thickness by ellipsometry. Rotating disks and rotating concentric cylinders also provide well-characterized fluid flow with uniform mass transfer; however they cannot be used for *in-situ* ellipsometry which requires a stationary electrode.

Determination of Hydrodynamic Constant. Characterization of the resistance of an inhibitor to removal by hydrodynamic forces requires knowledge of the hydrodynamic shear exerted on the metal surface. The shear is related to a hydrodynamic constant which is a function only of cell geometry and jet velocity. An experimental technique was developed[21] to obtain the hydrodynamic constant which involved the use of a ring electrode substituted for the copper disk in Figure 1. Under the assumptions of a large Schmidt number (valid for aqueous electrolytes) and a high concentration of supporting electrolyte, the hydrodynamic constant can be obtained from measurement of the mass-transfer-limited current on a ring electrode through

$$a = \frac{\rho}{\mu}\left\{\frac{s_i \mathrm{Sc}^{2/3} I}{0.85001\pi n F c_{i,\infty}\left(r_2^3 - r_1^3\right)^{2/3}}\right\}^2, \tag{4}$$

where n is the number of electrons transferred in the reaction, s_i is the stoichiometric coefficient for the reacting species i, F is Faraday's constant, I is the total current measured on the ring, $c_{i,\infty}$ is the bulk concentration of the mass-transfer-limiting species, and r_1 and r_2 are the inner and outer radii, respectively, of the ring electrode. Reduction of ferricyanide on nickel in 1.0M NaOH provides an excellent system for these experiments because this satisfies the assumptions given above and provides a broad limiting-current plateau which allows easy measurement of I. The ferricyanide diffusivity, which enters through the Schmidt number Sc, can be measured by means of rotating disk experiments. The solution density and viscosity, the bulk ferricyanide concentration, and the ring dimensions can also be measured independently. Results obtained with this system can be applied to corrosion in brine solutions because the hydrodynamic constant obtained through equation (4) is not a function of fluid properties.

For disk diameters of the same size as the nozzle diameter d ($r/d = 0.5$), the measured hydrodynamic constant was shown to be independent of radial position.[21] This result is independent of the distance between the nozzle and the electrode (h) in the range of $h/d = 1$ to $h/d = 5$. Different points of departure from stagnation region flow have been reported in the literature. Coueret[25] reported that stagnation flow extended to $r/d = 1.4$ for turbulent cicular jets; whereas Chin and Tsang[16] reported that the critical radius should be revised to $r/d = 1.0$. Both used electrochemical reduction of ferricyanide on disk electrodes rather than ring electrodes as used here. The discrepancy between their results and those obtained in our laboratory is probably due to physical differences between the two methods. A disk electrode that is large enough to extend into the region where stagnation flow theory does not apply still has a significant portion of the disk in the stagnation flow region. In contrast, a ring electrode can be constructed to lie wholly inside or outside the stagnation region. The ring electrode measurements are therefore more sensitive to changes in the flow pattern.

The ring electrode measurements were used to identify the appropriate dimensions for the disk electrode that would ensure the existence of well–defined flow. A series of ring electrode experiments were also used to obtain the hydrodynamic constant as a function of jet velocity. The local shear stress can therefore be calculated as a function of radial position from equation (3), with viscosity μ and density ρ measured with a viscometer and a hydrometer, respectively. This information, coupled with the technique illustrated in Figure 4, allows determination of the shear stress at points of morphological changes on a disk electrode.

Corrosion of Copper in Saline Solutions

The corrosion of a rotating copper disk is being studied in aerated and deaerated 0.5M NaCl solutions as a function of applied potential, pH, and rotation rate. This work is intended to provide a foundation for the study of the influence of large values of hydrodynamic shear. The electrochemical techniques include A.C. impedance spectroscopy and potentiodynamic and potentiostatic experiments. The potentiostatic experiments reveal a significant effect of rotation speed at potentials greater than 0.5 V(SCE). The may be associated with removal of a precipitated film which, at this potential, was loosely adherent. Salt films and oxide layers were observed on the electrode surface, and these appeared either as rings growing inward with increasing potential from the periphery of the disk or as circles growing radially outward from the center. These observations can be explained in terms of the potential and current distributions expected on a disk electrode below the limiting current.[17] Rings growing inward observed during the corrosion of iron in sulfuric acid have been shown to be caused by deposition of ferrous sulfate salts.[26] The ring observed at low potentials may be associated with deposition of $CuCl_2$ which is sparingly soluble. The circles observed are probably associated with formation of copper oxides (see reference 27). This work, augmented with chemical and microscopic analyses of the corrosion products, will continue throughout the next year both for copper and for model alloys.

Preparation of Copper–Aluminum Alloys

Aluminum bronzes are of two general types: the α or single–phase alloys, often referred to as homogeneous alloys, and the α–β, or two–phase alloys, known as duplex bronzes. Under perfect equilibrium conditions 9.8 percent of Al is soluble in Cu before the β phase appears, but, in practice, alloys containing in excess of 7.5 percent Al usually exhibit two phases.[28] Since the properties of the α–β alloys differ from those of the single phase, the duplex bronzes will not be prepared at this point. Also, under certain conditions of corrosion the α–β aluminum bronzes are susceptible to dealuminization.[28]

The alloys were melted in an induction furnace located in the Department of Materials Science at the University of Virginia. The induction coils of the furnace are concentrated near the bottom of the crucible, thus causing a temperature gradient in the crucible. To compensate for its higher melting point (1083°C as compared to 660°C for aluminum), the copper is placed at the bottom of the crucible where it melts first. The aluminum is placed on the copper where it receives less heat. The molten mixture is stirred by rocking

the crucible for five minutes. A homogeneous composition and temperature distribution is obtained when the color of the melt matches that of the crucible (white). Care must be taken to avoid excessive temperatures which will cause loss of aluminum by vaporization. Some loss of aluminum will occur even under optimal conditions. The melt is then poured into a mold and slowly cooled. Impurities collect at the top of the mold, and this metal is therefore be cut and discarded. The resulting ingot is rolled, homogenized at about 800°C, cut turned, and annealed according to ASM standards.[29,30] Samples will be sent to outside laboratories to provide confirmation of alloy composition through chemical analysis. The samples prepared in this way will be machined to form electrodes for electrochemical and *in-situ* ellipsometric studies.

Plans for Next Years Research

Our short-term plans for this work include:

- to conduct preliminary experiments with copper in saline solutions to study the growth and removal of passive films under high-shear flow by the new ellipsometer system,
- to conduct electrochemical studies of rotating copper disk electrodes in aerated and deaerated neutral and basic saline solutions to identify the conditions for passivation in the absence of erosive effects, and
- to conduct parallel rotating disk studies of copper alloys in aerated and deaerated neutral and basic saline solutions to identify the effect of alloy composition on passivation in the absence of erosive effects.

Acknowledgement

This work is supported by the Office of Naval Research under Contract Number: N00014-87-K-0042. The support of Dr. A. John Sedriks is gratefully acknowledged.

References

1. R. B. Bird, W. E. Stewart, and E. N. Lightfoot, *Transport Phenomena,* John Wiley and Sons, Inc., New York, 1960.

2. H. Schlichting, *Boundary–Layer Theory,* McGraw-Hill Book Co., New York, 1968.

3. R. W. Fahien, *Fundamentals of Transport Phenomena,* McGraw-Hill Book Co., New York, 1983.

4. H. R. Copson, "Effects of Velocity on Corrosion," *Corrosion* **16** (1960), 86t-92t.

5. K. D. Efird, "Effect of Fluid Dynamics on the Corrosion of Copper-Based Alloys in Seawater," *Corrosion* **33** (1977), 3-8.

6. F. Giralt, and O. Trass, "Mass Transfer from Crystalline Surfaces in a Turbulent Impinging Jet: Part I. Transfer by Erosion," *Canadian Journal of Chemical Engineering* **53** (1975), 505-511.

7. L. R. Steele, and C. J. Geankoplis, Mass Transfer from a Solid Sphere to Water in Highly Turbulent Flow," *AIChE Journal* **5** (1959), 178-181.

8. D. C. Silverman, "Rotating Cylinder Electrode for Velocity Sensitivity Testing," *Corrosion* **40** (1984), 220-226.

9. D. B. Anderson, and K. D. Efird, "The Influence of Chromium on the Corrosion Behavior of Copper-Nickel Alloys in Seawater," *Proceedings of the 3rd International Congress on Marine Corrosion and Fouling,* National Bureau of Standards, Gaithersburg, MD, October 2-6, 1972, 264-276.

10. P. T. Gilbert, and F. L. Laque, "Jet Impingement Tests," *Journal of the Electrochemical Society* **101** (1954), 448-455.

11. D. A. Jones, "Effect of Water Chemistry on the Erosion–Corrosion of Aluminum in High Temperature High Velocity Water," *Corrosion* **37** (1981), 563-569.

12. M. T. Scholtz, and O. Trass, "Mass Transfer in a Nonuniform Impinging Jet: Part I. 'Stagnation Flow–Velocity and Pressure Distribution," *AIChE Journal* **16** (1970), 82-90.

13. M. T. Scholtz, and O. Trass, "Mass Transfer in a Nonuniform Impinging Jet: Part II. Boundary Layer Flow-Mass Transfer," *AIChE Journal* **16** (1970), 90-96.

14. F. Giralt, C.-J. Chia, and O. Trass, "Characterization of the Impingement Region in an Axisymmetric Turbulent Jet," *Industrial and Engineering Chemistry, Fundamentals* **16** (1977), 21-28.

15. C.-J. Chia, F. Giralt, and O. Trass, "Mass Transfer in Axisymmetric Turbulent Impinging Jets,"*Industrial and Engineering Chemistry, Fundamentals* **16** (1977), 28-35.

16. D.-T. Chin, and C.-H. Tsang, "Mass Transfer to an Impinging Jet Electrode," *Journal of the Electrochemical Society* **125** (1978), 1461-1470.

17. J. Newman, "Current Distribution on a Disk Electrode Below the Limiting Current," *Journal of the Electrochemical Society* **113** (1966), 12351241.

18. J. M. Esteban, M. Lowry, and M. E. Orazem, "Correction of Experimental Data for the Ohmic Potential Drop Corresponding to a Secondary Current Distribution on a Disk Electrode," (invited paper) presented at the ASTM Symposium on Ohmic Electrolyte Resistance Measurement and Compensation, Baltimore, Maryland, May 19, 1988.

19. J. M. Esteban, M. Lowry, and M. E. Orazem, "Correction of Experimental Data for the Ohmic Potential Drop Corresponding to a Secondary Current Distribution on a Disk Electrode," submitted for an *ASTM Special Technical Publication on Ohmic Electrolyte Resistance Measurement and Compensation.*

20. Marc M. Lowry, *The Corrosion of Iron in Acidic Chloride Solutions,* M.S. thesis, University of Virginia, January 1988.

21. G. Hickey and M. E. Orazem, "An Experimental Technique for Evaluating Film Persistency," Paper #449 presented at Corrosion/87, Annual Conference of the National Association of Corrosion Engineers, San Francisco, California, March 13, 1987.

22. G. Hickey, J. M. Esteban, and M. E. Orazem, "An Experimental Technique for Evaluating Film Persistency," *Corrosion,* reviewed and revised.

23. J. Matthew B. Esteban, *Evaluation of Inhibitor Film Persistency in Air–Saturated Acidic Chloride Solutions,* M.S. thesis, University of Virginia, August 1988.

24. C. B. Diem and M. E. Orazem, "A Scanning Ellipsometer to Evaluate the Influence of Fluid Velocity on Corrosion," presented at the T–5A Workshop on Fluid Flow Enhanced Corrosion, Corrosion/88, Saint Louis, Missouri, March 21–25, 1988.

25. F. Couret, "Transfert de Mateire Lois de l'Impact Normale de Jets Liquides Circulares Immerges," *Chemical Engineering Science* **30** (1975), 1257–1263.

26. M. E. Orazem and M. G. Miller, "Current Distribution and Formation of a Salt Film on an Iron Disk Below the Passivation Potential," *Journal of the Electrochemical Society* **134** (1987), 392–399.

27. M. Pourbaix, *Atlas of Electrochemical Equilibria in Aqueous Solutions,* National Association of Corrosion Engineers, Houston, Texas, 1974, p384.

28. R. A. Wilkins and E. S. Bunn, *Copper and Copper Based Alloys,* McGraw–Hill Book Co., New York, 1943, p253.

29. "Foundry Melting of Copper Alloys," *Metals Handbook,* 8th edition, volume 5, ASM, Metals Park, Ohio, 1964, p416.

30. "Heat Treating of Copper and Copper Alloys," *Metals Handbook,* 8th edition, volume 2, ASM, Metals Park, Ohio, 1964, p284.

Appendix A: Papers Supported by this Contract

- J. M. Esteban, M. Lowry, and M. E. Orazem, "Correction of Experimental Data for the Ohmic Potential Drop Corresponding to a Secondary Current Distribution on a Disk Electrode," (invited paper) presented at the ASTM Symposium on Ohmic Electrolyte Resistance Measurement and Compensation, Baltimore, Maryland, May 19, 1988. Also submitted for the *ASTM Special Technical Publication on Ohmic Electrolyte Resistance Measurement and Compensation.**

* This work was supported in part by the Chemicals and Metals Department, DOW Chemical, USA, by the Institute for Materials Science and Engineering of the Virginia Center for Innovative Technology, Grant No. MAT-86-028, and by the Office of Naval Research under Contract Number N00014-87-K-0042.

Correction of Experimental Data for the Ohmic Potential Drop Corresponding to a Secondary Current Distribution on a Disk Electrode*

J. Matthew Esteban, Marc Lowry, and Mark E. Orazem
Department of Chemical Engineering
University of Virginia
Charlottesville, Virginia 22901

June 9, 1988

Abstract

A numerical method is presented for adjusting experimental current–potential curves for the Ohmic resistance corresponding to a secondary current distribution on a (rotating) disk electrode. The nonuniform current and potential distributions on the disk electrode cause the electrolyte resistance itself to be a function of measured current. The method described here is employed after experiments are conducted and yields the Tafel slope as well as adjusted values for current density and surface overpotential that apply to the center of the disk. This facilitates comparison of experimental data to mathematical models of the rotating disk electrode that, in the secondary current regime, apply strictly only to the center of the electrode. The Tafel slopes obtained agree to within 3 mV/decade with standard techniques for Ohmic correction such as current interruption because, at the high current densities where the Ohmic correction is most significant, the resistance correction approaches the primary resistance obtained by current interruption. The Tafel slope values for the two methods differ most for solutions of low conductivity. The major advantages of the Ohmic correction method described here are that the experimental condition is never perturbed and that the method indicates the extent to which the current distribution is nonuniform.

The reaction mechanisms governing an electrochemical systems are commonly identified through comparison of experimentally determined Tafel slopes or apparent transfer coefficients to "theoretical values" obtained from simplifications of specific reaction mechanisms. Analysis of experimental data must include treatment of the contribution to the measured potential from the electric resistance of the electrolyte, a term that can be significant at

* presented at the *ASTM Symposium on Ohmic Electrolyte Resistance Measurement and Compensation,* Baltimore, Maryland, May 17, 1988 and submitted for an *ASTM Special Technical Publication on Ohmic Electrolyte Resistance Measurement and Compensation.*

large currents or in dilute solutions of low conductivity. A number of techniques are available for making this correction. The Ohmic contribution, for example, can be reduced but not eliminated through close placement of reference electrodes to the working electrode. A disadvantage of this approach is that exact placement of the reference electrode is critical, and uncertainty in the electrode location can be a significant source of error. Another approach is to place the reference electrode sufficiently far from the working electrode that the distance can be considered to approach infinity. This allows use of mathematical calculation of the Ohmic contribution to the measured potential. Current interruption can also be used to obtain the Ohmic contribution to the cell potential.

The object of this paper is to describe a numerical technique used by Lowry[1,2] to correct polarization data for the Ohmic resistance corresponding to a secondary current distribution on a disk electrode. This procedure was suggested by Newman in his analysis of the current and potential distribution on a rotating disk electrode.[3,4] The treatment presented here has the advantages that it does not require perturbation of the electrochemical system and that it takes into account the nonuniform current and potential distribution present on a disk electrode in the Tafel regime. The analysis can therefore be used to determine the extent to which the coupling of Ohmic and kinetic effects cause the current distribution on the electrode to be nonuniform. This information could facilitate interpretation of spatial variations of surface morphology or of electrode profiles after corrosion experiments. Use of this technique is restricted to a disk electrode with a reference electrode located infinitely far away and at currents below values where mass-transfer effects are seen. Accurate values of solution conductivity and disk radius are also needed. The Tafel slopes are estimated by an iterative procedure utilizing data within the Tafel region where the Ohmic resistance typically cannot be neglected.

A brief discussion on the use of polarization measurements to measure corrosion rates and Tafel slopes is presented. The method is illustrated through analysis of data taken by

Lowry *et al.*,[2] and the results are compared to those obtained from other Ohmic compensation methods.

Theoretical Development

Analysis of experimental data is usually based on simplification of the general Butler–Volmer kinetic expression. The discussion here follows the Butler–Volmer expression, a summary of Newman's analysis of the secondary current distribution on a disk electrode, and the numerical method developed for Ohmic compensation.

Identification of Tafel Parameters

The rate at which reversible electrochemical reactions proceed can be described by a Butler-Volmer type equation:

$$i = i_o \left\{ \exp\left(\frac{\alpha_a F}{RT} \eta_s \right) - \exp\left(-\frac{\alpha_c F}{RT} \eta_s \right) \right\}. \tag{1}$$

The current density i is the sum of the anodic and cathodic contributions where i_o is the exchange current density, α_a and α_c are the apparent anodic and cathodic transfer coefficients, respectively, and η_s is the surface overpotential. The kinetic parameters i_o, α_a, and α_c can be determined from experimental data through use of Equation (1). The exchange current density is a function of the electrolyte composition adjacent to the electrode surface and is large for reactions that are fast or reversible.[5] The surface overpotential provides the driving force for the reaction and is a measure of departure from the equilibrium potential Φ_{eq} . For reversible reactions, Φ_{eq} is given by the Nernst equation.

Electrode kinetic studies are performed by applying an external potential Φ_{app} such that

$$\Phi_{app} = \Phi_{eq} + \eta_s + \Phi_o + \eta_c . \tag{2}$$

These potentials are measured relative to a known potential of a reference electrode such as the saturated calomel electrode (SCE). The concentration overpotential η_c is due to changes in concentration and conductivity at the electrode surface relative to the bulk. This term can be neglected for currents sufficiently below the limiting current and will not be treated in this work. The Ohmic potential drop Φ_o is attributed to the solution resistance and is a measure of the driving force necessary to pass current through the electrolyte. At low current densities and close to the equilibrium potential, Φ_o is negligible; the contrary is true at high currents. The objective of the Ohmic compensation techniques discussed here is to identify the current–potential characteristics of a given system in the absence of this term.

When the surface overpotential becomes large, either the anodic or cathodic current dominates. Equation (1) reduces to an expression where the surface overpotential becomes linear with respect to the logarithm of the current density. This is called the Tafel region, and polarization within this regime is essentially activation controlled. In the anodic Tafel region

$$\eta_s = \frac{2.303RT}{\alpha_a F} \log\left(\frac{i}{i_o}\right) = a_a + b_a \log i, \tag{3}$$

where

$$a_a = -\frac{2.303RT}{\alpha_a F} \log i_o,$$

and the anodic Tafel slope (in units of V/decade) is given by

$$b_a = \frac{2.303RT}{\alpha_a F}.$$

Analogous expressions for the cathodic Tafel region can be obtained.

Tafel extrapolations can also be applied to corrosion reactions through use of mixed-potential theory.[6] The basis of the polarization techniques found in the literature[7-15] for

evaluating kinetic parameters is that the current density for a corroding system consisting of individual reversible reactions can be approximated by

$$i = i_{corr}\left\{\exp\left(\frac{2.303\,\eta_s}{b_a}\right) - \exp\left(-\frac{2.303\,\eta_s}{b_c}\right)\right\}, \tag{4}$$

where the surface overpotential is defined to be

$$\eta_s = \Phi_{app} - \Phi_{corr} - \Phi_o, \tag{5}$$

and i_{corr} and Φ_{corr} are the corrosion current and corrosion potential, respectively. The corrosion potential has a value between the reversible potentials of the individual reaction pairs. The principal assumption inherent in Equation (4) is that the major contributors to the overall current are the metal dissolution reaction and the reduction of some electroactive species. For this approximation to be valid, Φ_{corr} must be sufficiently far from the two reversible potentials.[8]

The techniques described in References [7] to [15] utilize current–potential data in the pre–Tafel region. The measurements are performed at low currents and close to Φ_{corr} where the Ohmic contribution to the potential in Equation (5) is negligible. The experimental data are fitted into Equation (4) to yield values for i_{corr}, b_a, b_c, and/or Φ_{corr}. The methods of Mansfeld and co-workers[8-12] for analyzing polarization data and Barnartt's three–point method[13,14] and its variation[15] do not require assumption of a linear polarization curve near the corrosion potential.

The Secondary Current Distribution on a Disk Electrode

At large current densities, the contribution of the Ohmic potential drop to the applied potential must be considered. The Ohmic resistance is a function of the distance between the reference and working electrodes, the conductivity of the solution, and the geometry of the working electrode. Experimental errors in the measurement of Ohmic drop could

be reduced by setting the reference electrode at "infinity" with respect to the working electrode. The Ohmic resistance is insensitive to changes in the position of the reference electrode when the latter is placed relatively far from the working electrode.[3] This simplifies the experimental apparatus, *i.e.*, no Luggin capillary is necessary, and allows some leeway on electrode placement.

A procedure for Ohmic potential drop correction was derived from Newman's analysis of the current and potential distribution on a disk electrode.[3,4] The current distribution can be described as primary or secondary depending on the applied potential. The term Φ_{eq} can be neglected in Equation (2) when the applied potential is measured against a reference electrode of the same kind as the working electrode. The concentration overpotential η_c can also be neglected at high convection rates. Each of the remaining terms vary with radial position in order to maintain Φ_{app} constant over the entire disk.

A uniform potential in the solution adjacent to the electrode surface is obtained when both η_c and η_s are negligible. In this regime, the reaction rate constants are high and the current distribution is determined by the Ohmic drop through the solution. The primary current distribution on an equipotential surface is

$$i = \frac{0.5\, i_{avg}}{\sqrt{1-(r/r_o)^2}}, \tag{6}$$

and the primary resistance is given by

$$\Phi_o = \frac{I}{4\,\kappa_\infty\, r_o}, \tag{7}$$

where I represents the total current, κ_∞ is the solution conductivity, and r_o is the radius of the disk electrode.[3]

The secondary current distribution applies when the surface overpotential cannot be neglected, and the current at a point on the electrode becomes a function of the potential of

the adjacent solution. The secondary current distribution under Tafel kinetics[4] is presented in Figure 1 as a function of radial position with $\beta\delta$ as the parameter where δ is given by

$$\delta = |i_{avg}| \frac{zFr_o}{RT\kappa_\infty}, \tag{8}$$

and represents the dimensionless average current density. For solutions with supporting electrolyte, z is defined to be equal to $-n$, the number of electrons transferred in the reaction. The term βz is the apparent cathodic or anodic transfer coefficient α_c or α_a. The current distribution is now determined by the requirement that the current at any location satisfy both Ohm's law, relating current to a gradient in potential at that location, and the kinetic expression relating current to the local value of the surface potential. This is in contrast to the primary case where the local value of current density need only satisfy Ohm's law. The potential in the solution for both primary and secondary distributions is governed by Laplace's equation. As $-\beta\delta$ tends toward ∞, the current distribution approaches the primary distribution where the current density approaches infinity at the disk edge and is equal to one–half the average current value at the center of the disk. As $-\beta\delta$ approaches zero, the current distribution becomes uniform. This means that kinetic limitations to the electrode reaction cause the current distribution to become more uniform and cause the potential adjacent to the electrode surface to deviate from a uniform value to overcome the tendency of current to favor the edge of the electrode.[4,5]

One consequence of the nonuniform secondary distribution for the potential of the solution adjacent to the electrode is that subtraction of the Ohmic correction for a primary distribution applies strictly only for a single radial position on the disk, and that the location of this position is a function of the average current density. One can, however, reference the Ohmic potential drop and the current density to values appropriate for the center of the disk. This approach requires that the Ohmic resistance be a function of the average current density. The primary Ohmic potential drop is therefore corrected by a factor given in Figure

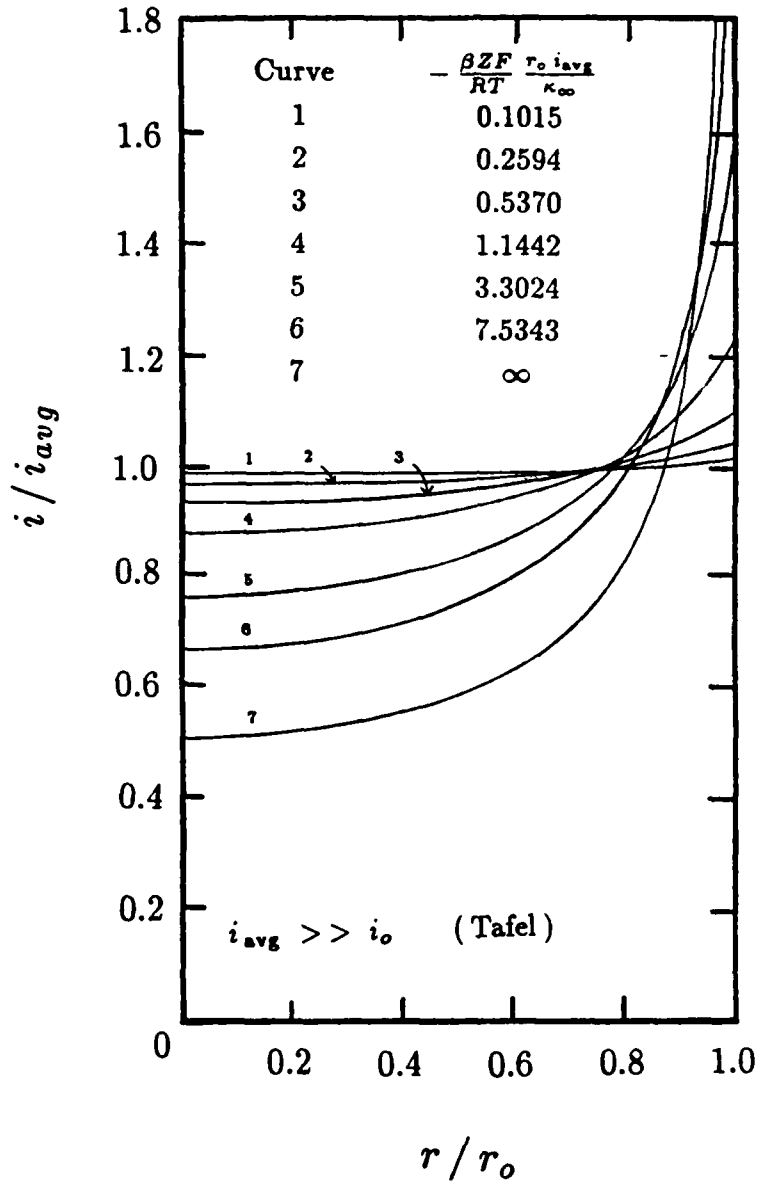

Figure 1: Secondary current distribution on a disk electrode for Tafel kinetics (following reference 4).

2 as a function of the ratio of the current density at $r = 0$ to the average current density. This factor is equal to unity for the primary current distribution (where the potential of the solution adjacent to the disk is uniform) and approaches 1.273 when the current distribution becomes uniform.

If one could obtain the ratio $i/i_{avg}\,|_{r=0}$ from Figure 1, the applied potential could be corrected for the Ohmic drop to obtain the surface overpotential at the center of the disk electrode, *i.e.*,

$$\eta_s\,|_{r=0} = \Phi_{app} - \Phi_o\,|_{r=0}, \tag{9}$$

or

$$\eta_s\,|_{r=0} = \Phi_{app} - \frac{I}{4\kappa_\infty r_o}\left[\left.\frac{\Phi_o\, 4\kappa_\infty r_o}{I}\right|_{r=0}\right], \tag{10}$$

where I is the total current to the disk at an applied potential Φ_{app} measured relative to a reference electrode. The term in the bracket is the correction factor for the primary resistance to the center of the disk electrode determined from Figure 2.

The Numerical Method for Ohmic Compensation

Data obtained from potentiostatic or potentiodynamic experiments may be corrected for Ohmic potential drop at the center of the disk to acquire the surface overpotential and current density at $r = 0$ using the procedure derived from Newman's treatment of the disk electrode. Reliable estimates for the Ohmic contribution can be obtained since the calculations are referenced to a radial position where the Ohmic potential drop and current density are known.

Values for $i/i_{avg}\,|_{r=0}$ from Figure 1 were plotted as a function of $|1/\beta\delta|$ to yield Figure 3. This plot shows that as $|1/\beta\delta| \rightarrow 10$ the current distribution becomes nearly uniform. Since

$$\frac{1}{\beta\delta} = \frac{RT\kappa_\infty}{\beta n F r_o\, i_{avg}}, \tag{11}$$

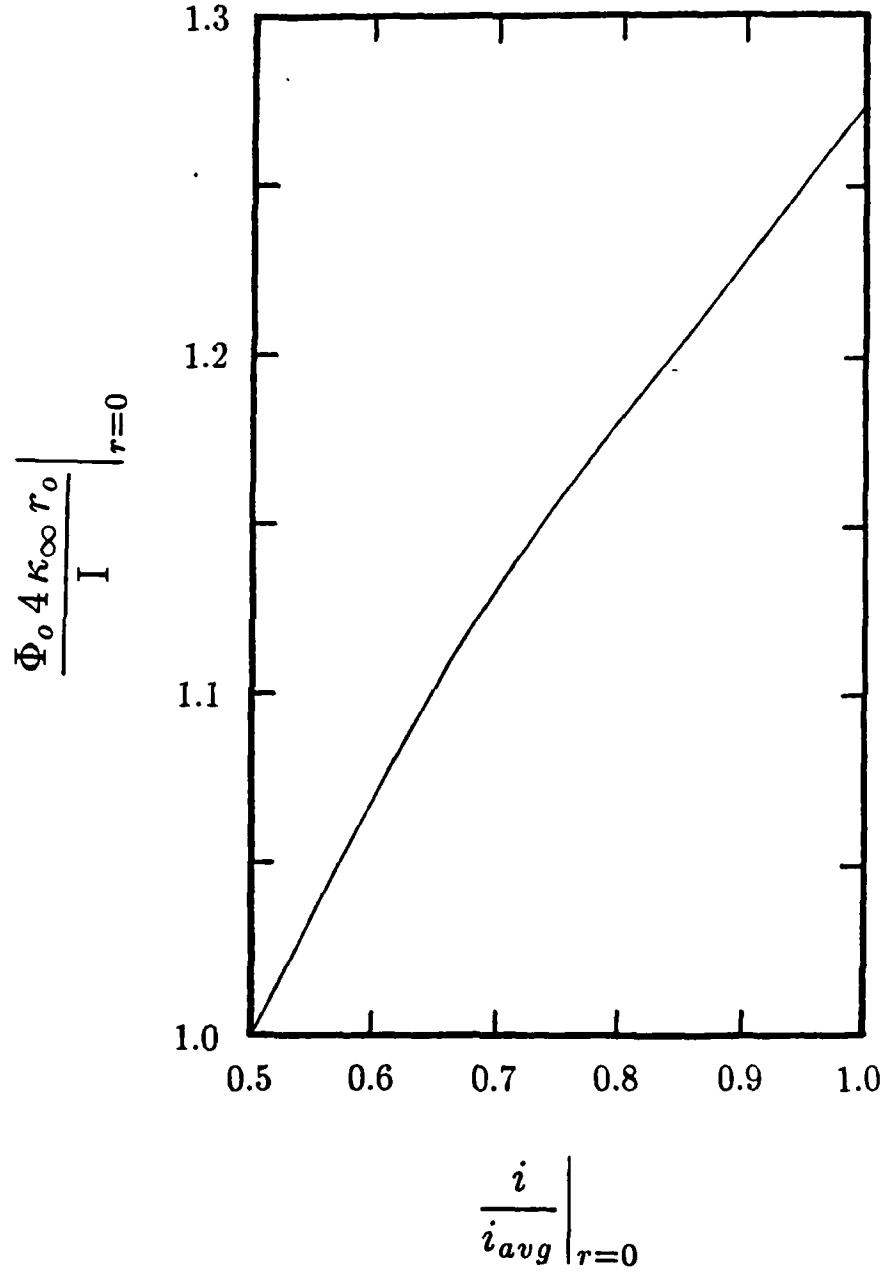

Figure 2: Correction factor for the primary resistance used to correct for the Ohmic potential drop to the center of the disk electrode under a secondary current distribution (following reference 4).

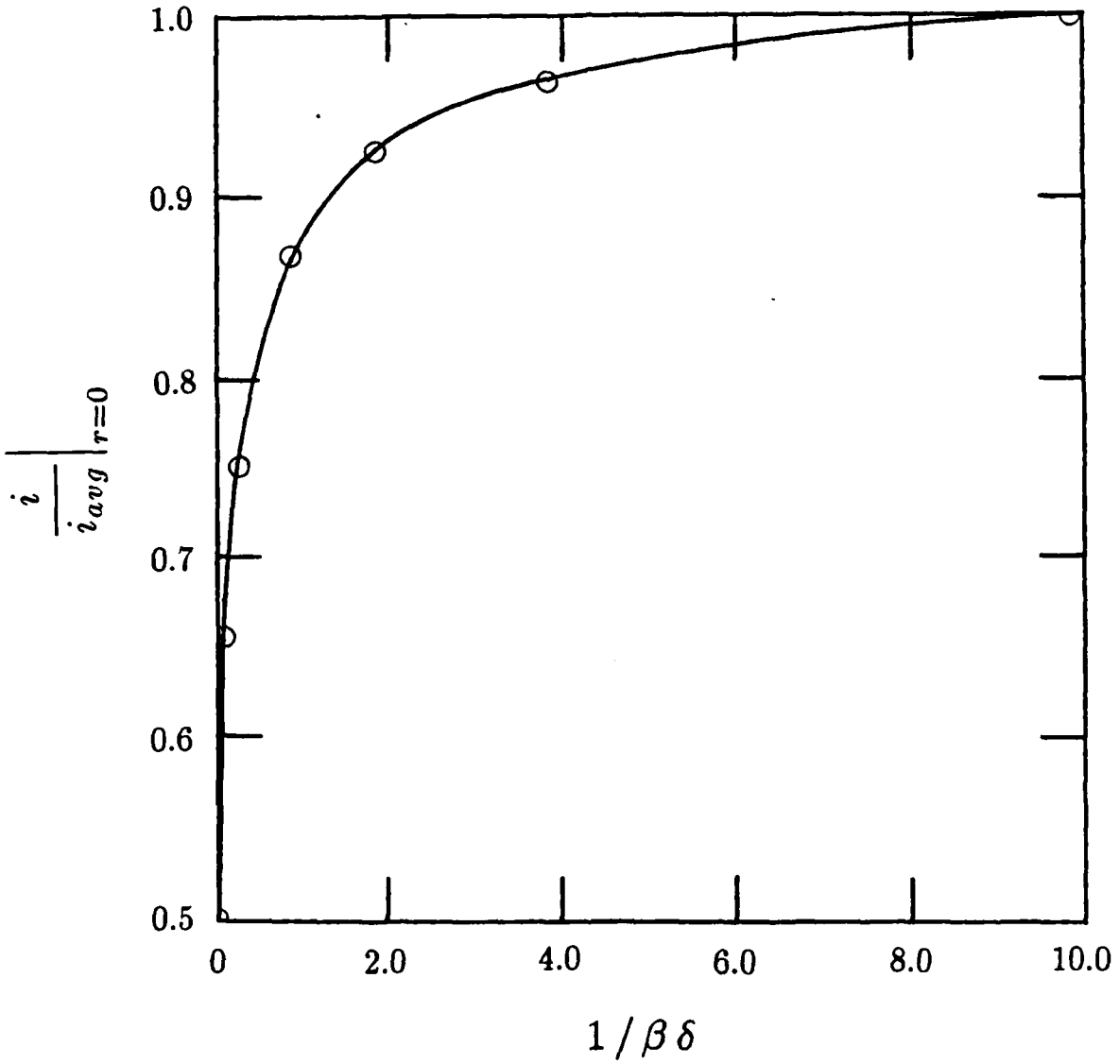

Figure 3: Correction factor for the average current density used to obtain the current density at the center of the disk electrode under a secondary current distribution.

an expression for β can be related to the Tafel slope obtained from Newman's expression relating the current density to the surface overpotential. Therefore,

$$b = \frac{2.303\,RT}{\beta\,n\,F}, \tag{12}$$

or

$$\beta = \frac{2.303\,RT}{b\,n\,F}. \tag{13}$$

With

$$i_{avg} = \frac{I}{\pi\,r_o^2}, \tag{14}$$

Equation (13) becomes

$$\frac{1}{\beta\delta} = \frac{b\,\kappa_\infty\,\pi\,r_o}{2.303\,I}. \tag{15}$$

The iterative procedure to obtain $\eta_s\,|_{r=0}$ requires an initial guess for the Tafel slope and calculation of the parameter $1/\beta\delta$ from Equation (15) for each pair of current-potential data. The corresponding value of $i/i_{avg}\,|_{r=0}$ is subsequently obtained from a discretized version of Figure 3. The correction factor for the primary resistance at the center of the disk electrode is estimated from a curve-fit of Figure 2, and the surface overpotential at $r = 0$ is calculated from Equation (10). A new value for the Tafel slope is determined from linear regression of the adjusted data plotted as $\eta_s\,|_{r=0}$ versus $\log(i\,|_{r=0})$ where

$$i\,|_{r=0} = \left[\frac{I}{\pi\,r_o^2}\right]\left[\left.\frac{i}{i_{avg}}\right|_{r=0}\right]. \tag{16}$$

This procedure is repeated until the error criterion for the Tafel slope is achieved. A flowchart describing the algorithm is presented as Figure 4. The computer program prepared for this method is documented in Reference [1].

A unique feature of this method is that the current distribution existing on a disk surface can be inferred from the corrected polarization data. The value of $i/i_{avg}\,|_{r=0}$ at

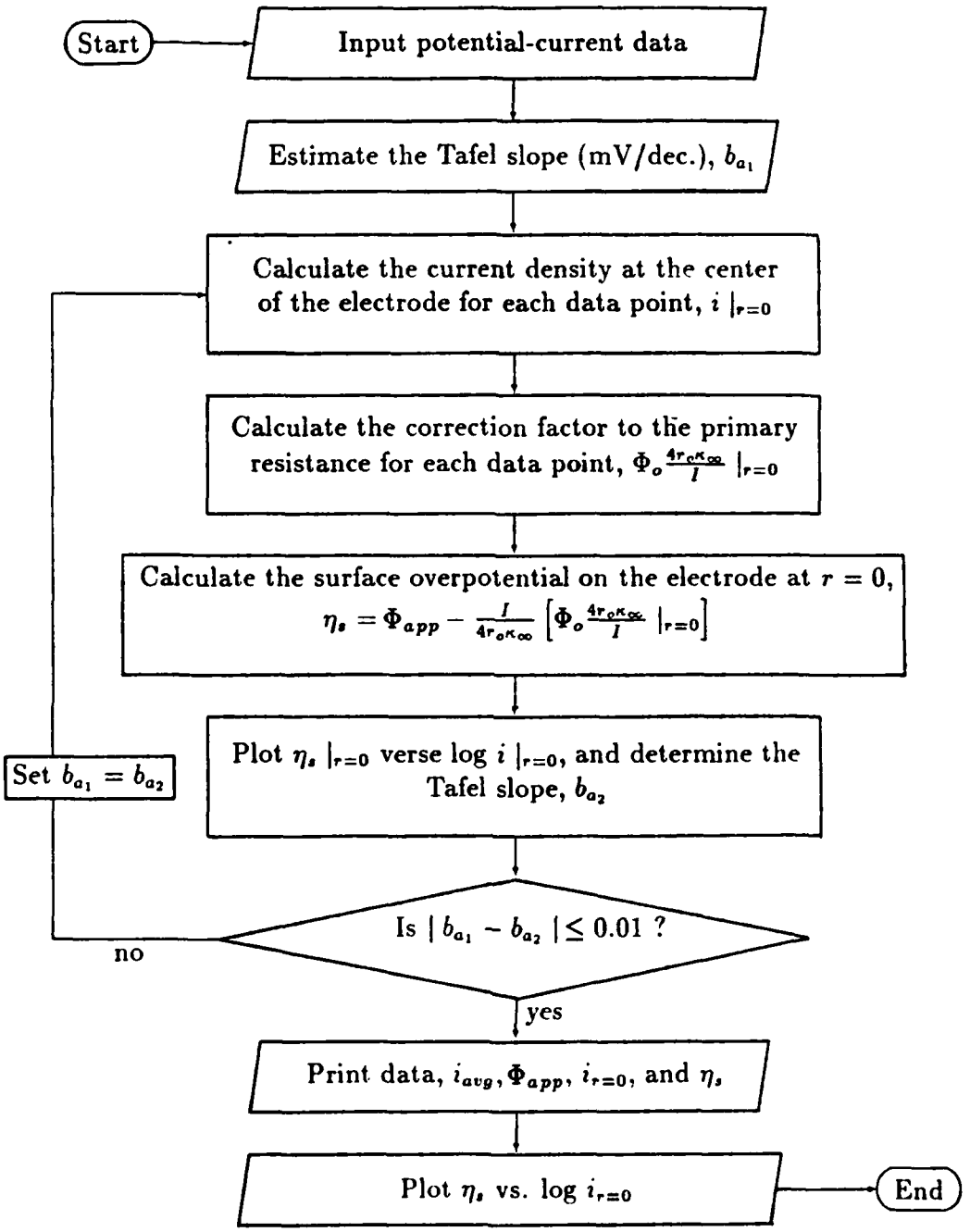

Figure 4: The flowchart describing the Ohmic drop correction algorithm.

a given potential can be compared with Figure 1. As this ratio approaches 1.0, a nearly uniform current distribution exists at the disk surface. Nonuniformities at the edge become discernable for $i/i_{avg}|_{r=0} < 0.95$.

Experimental Results

The use of this Ohmic correction program is illustrated here in the analysis of current–potential data acquired potentiostatically for the dissolution of iron in deaerated acidic chloride solutions.[1,2] These data are presented in Figures 5, 6, and 7 for chloride concentrations of 0.1 M, 1.0 M, and 4.5 M, respectively, in aqueous solutions with pH adjusted with HCl. The data points correspond to potentiostatic data obtained for individually polished electrodes held at the applied potential for between 15 to 45 minutes. These data are also shown as corrected by the iterative technique developed here. The Ohmic correction procedure yielded a Tafel slope value of 39 mV/decade for the 0.1 M Cl^- system, while the higher concentrations of 1.0 M and 4.5 M Cl^- gave values of 58 and 60 mV/decade, respectively. These are consistent with reported results (see, for example, references 1 and 2).

The correction of data for the Ohmic resistance by Newman's method was compared to that which would have been obtained by the current–interrupt technique. The Ohmic drop measured by the current–interrupt technique corresponds to the primary resistance of the system being studied.[16] This is a consequence of the small time constant for the interruption which does not allow time for discharge of the nonuniformly charged double layer associated with a *non–primary* current distribution. Therefore, to estimate the correction for the interrupter technique, the primary resistance was subtracted from the applied potential to give the surface overpotential, and the measured current was divided by the electrode surface area to get the average current density. The results of this correction to the data are also shown in Figures 5 through 7. The Tafel values based on the current–interrupt method differ by only 3 mV/decade for the 0.1 M Cl^- solution and the agreement improves

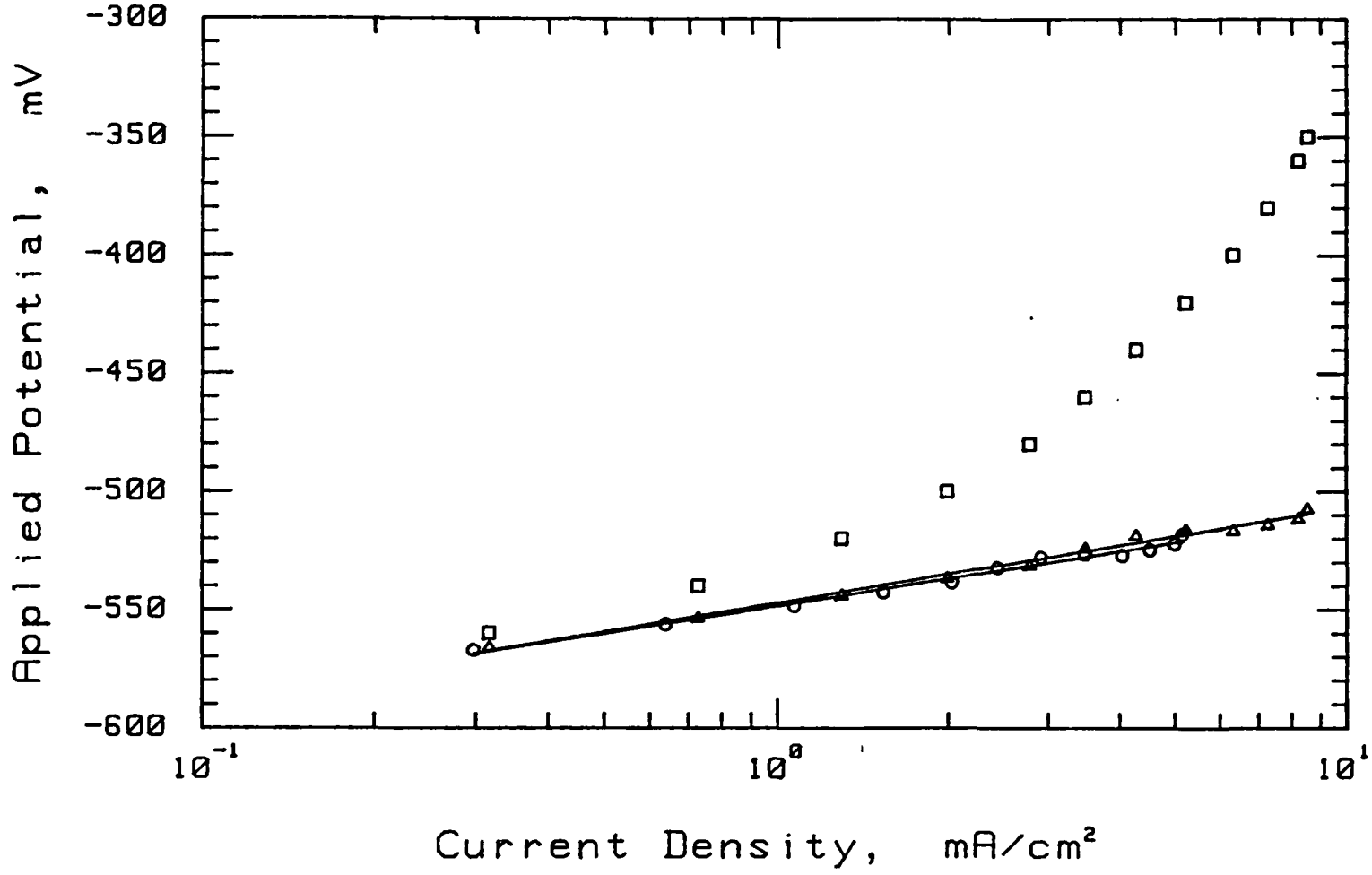

Figure 5: Tafel plot for measured current density as a function of applied potential for the corrosion of an iron disk in a 0.1 M Cl^- solution with a pH of 2. □, raw data, *i.e.*, averaged current density as a function of measured potential; ○, data corrected by the iterative program, *i.e.*, current density as a function of overpotential appropriate for the center of the disk electrode; and △, averaged current density as a function of overpotential obtained by a primary resistance correction, *i.e.*, the current–interrupt method.

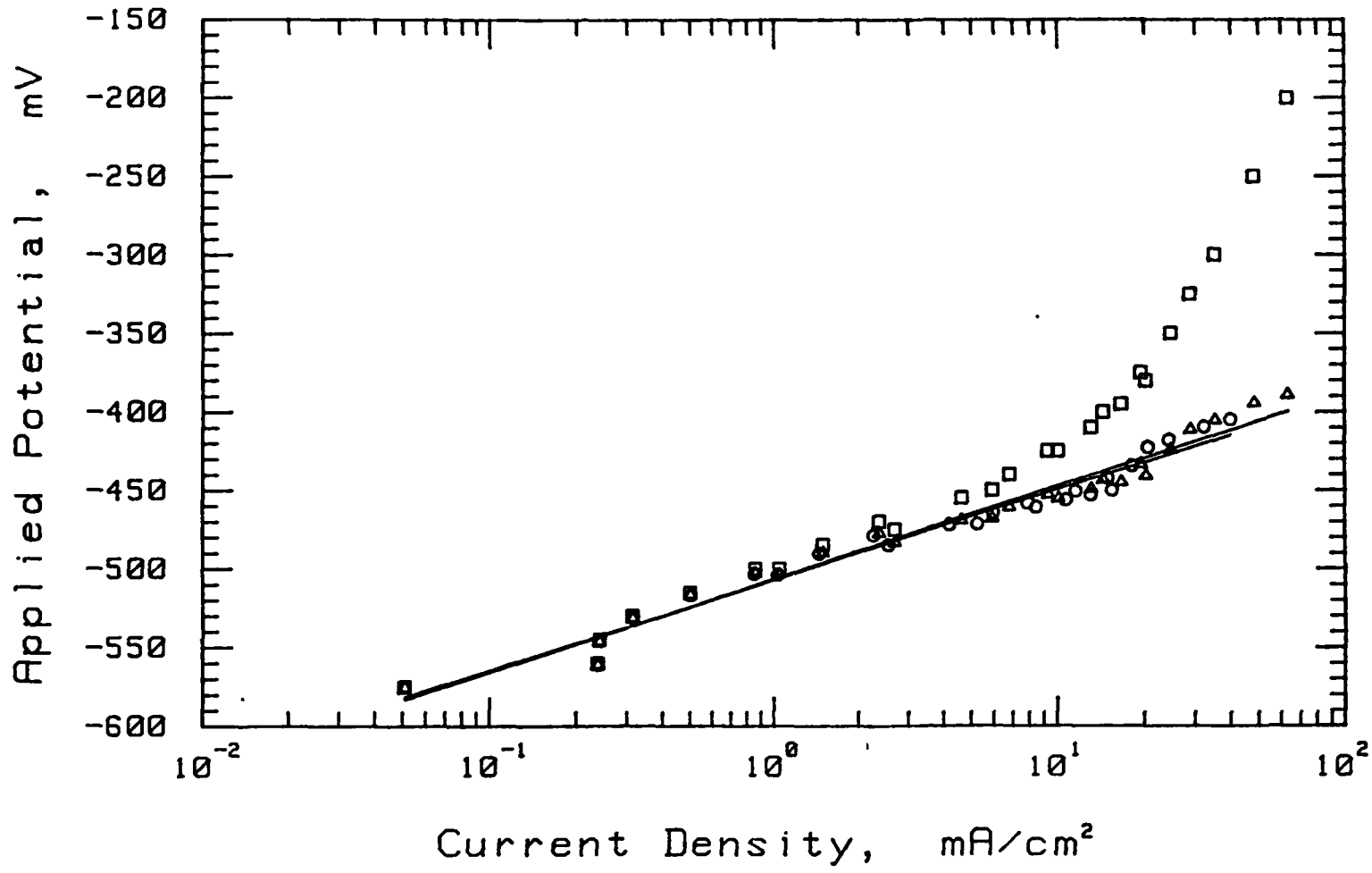

Figure 6: Tafel plot for measured current density as a function of applied potential for the corrosion of an iron disk in a 1.0 M Cl^- solution with a pH of 2. □, raw data, *i.e.*, averaged current density as a function of measured potential; ⊙, data corrected by the iterative program, *i.e.*, current density as a function of overpotential appropriate for the center of the disk electrode; and △, averaged current density as a function of overpotential obtained by a primary resistance correction, *i.e.*, the current–interrupt method.

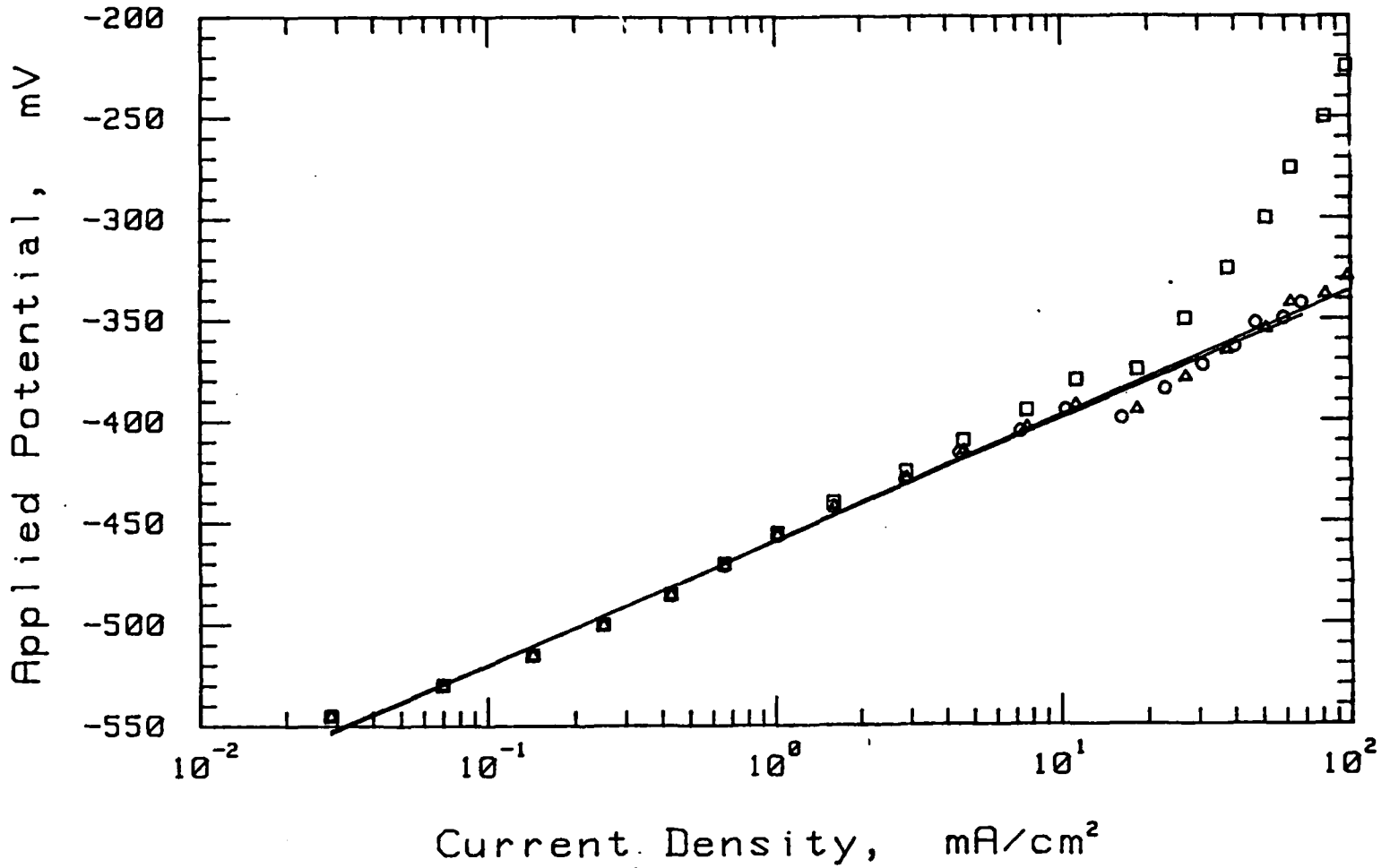

Figure 7: Tafel plot for measured current density as a function of applied potential for the corrosion of an iron disk in a 4.5 M Cl^- solution with a pH of 2. □, raw data, *i.e.*, averaged current density as a function of measured potential; ⊙, data corrected by the iterative program, *i.e.*, current density as a function of overpotential appropriate for the center of the disk electrode; and △, averaged current density as a function of overpotential obtained by a primary resistance correction, *i.e.*, the current–interrupt method.

as the Cl^- concentration increases. The difference is greater at lower conductivities because the Ohmic solution resistance is larger under these conditions.[16,17] Close agreement is seen because the Ohmic correction factor approaches one at the high current densities where Ohmic resistance is most significant. The variation of the calculated correction factor as a function of $\Phi_{app} - \Phi_{corr}$ is presented in Figure 8 for the three cases considered. The approach to a primary resistance at large overpotentials (or currents) is most apparent for the more dilute solutions where the Ohmic correction is most important. At lower current densities the small total current makes the Ohmic portion of the applied potential negligible, hence the surface overpotential is determined largely by the applied potential.

This correction procedure requires accurate values for the solution conductivity and electrode diameter. At the lower conductivities, such as those observed for the 0.1 M Cl^- solution, the magnitude of the Tafel slope was found to have a strong dependence on the value of the conductivity. A variation of 0.0005 $\Omega^{-1}cm^{-1}$ (4 percent) in κ_∞ caused a variation in the calculated Tafel slope of as much as 20 mV/decade. At higher concentrations, small changes in the conductivity had little influence on the Tafel slope. The conductivities used in the calculations presented here were obtained in independent experiments.

The "tangent method" described by Asakura and Nobe[18] was also employed. The polarization data were fitted to a Tafel equation in which the surface overpotential was modified by an Ohmic term corresponding to a constant solution resistance. The anodic Tafel slopes obtained (40, 56 and 59 mV/decade for the 0.1 M, 1.0 M, and 4.5 M Cl^- systems, respectively) were comparable to those obtained through the iterative calculations.

Conclusions

The numerical technique for correcting polarization data for the Ohmic resistance corresponding to a secondary current distribution on a disk electrode provides a useful tool for analysis of experimental data. The analysis is conducted after data are taken and does

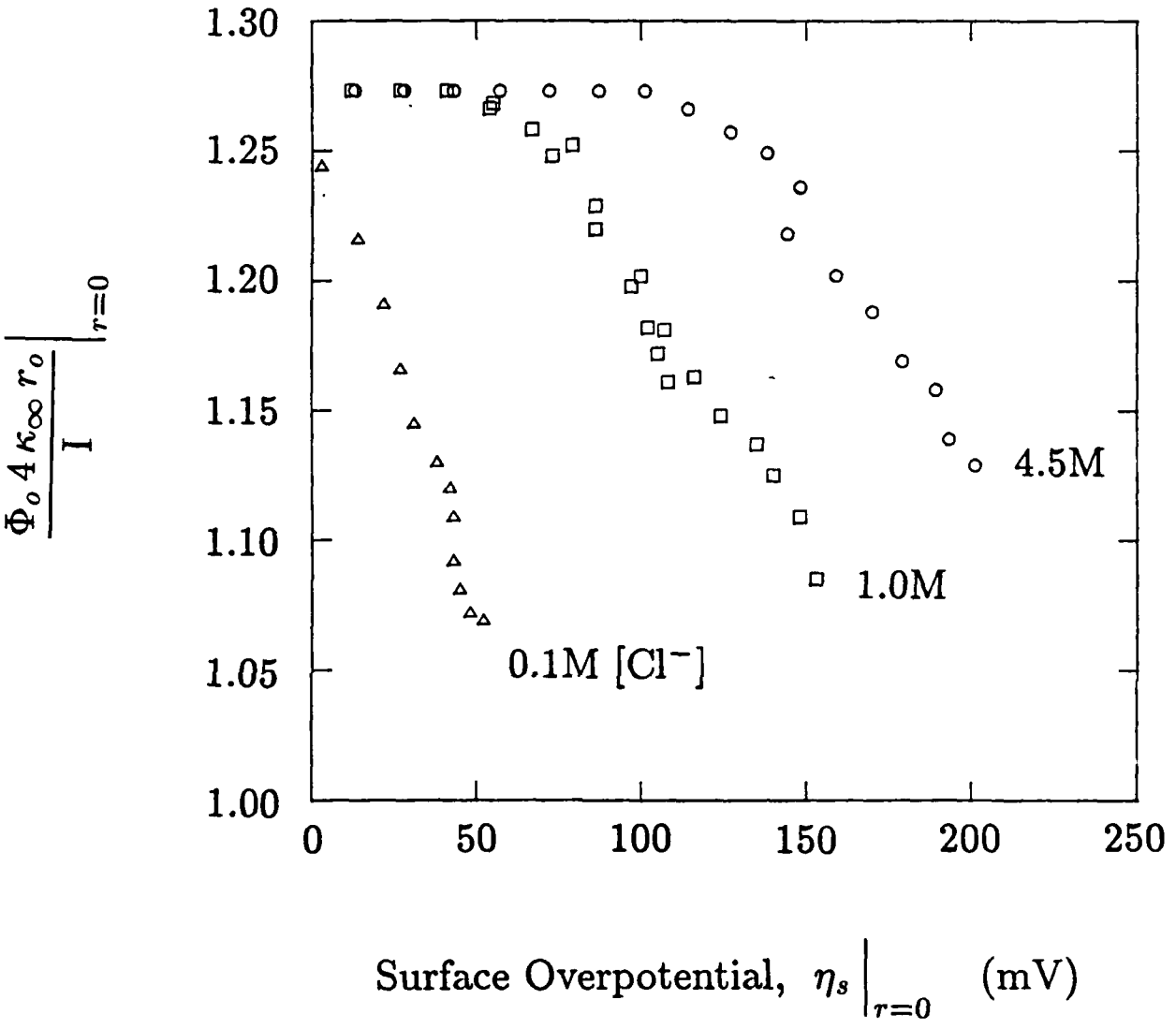

Figure 8: Correction factor for the primary resistance used to correct for the Ohmic potential drop to the center of the disk electrode under a secondary current distribution for △, 0.1 M Cl^- solution; □, 1.0 M Cl^- solution; and ○, 4.5 M Cl^- solution (see Figures 5, 6, and 7, respectively).

not require interruption of an experimental condition. This technique will be most useful when it is desireable to account for the nonuniform nature of the current and potential distribution at a disk electrode surface. The referencing of corrected current–potential data to the center of the disk is convenient for comparison to the results of one–dimensional models of rotating disks, and the results of the correction procedure provide information on the current distribution and the extent of nonuniformity across the disk electrode. This information cannot be obtained from other Ohmic potential compensation procedures. As can be done with other Ohmic correction techniques, the results of the correction can be used to obtain i_{corr} and Φ_{corr} through Tafel extrapolation of anodic and cathodic regions. The values obtained for Tafel slopes and corrosion current densities and potentials are in close agreement with other Ohmic correction techniques such as current–interruption.

The time required for calculation on a microcomputer is not excessive. Iterative treatment of 3000 data pairs with a program written in interpretive BASIC 4.0 on an HP–310 computer requires about 3 minutes, and treatment of 25 data pairs requires only a few seconds. The time required will be further reduced when the algorithm is rewritten in compiled Pascal. The use of this technique is restricted to the Tafel regime for cases where the rotation speed does not influence the measured current at a given applied potential and where the reference electrode is located far from the disk electrode. Accurate values are also needed for solution conductivity and electrode diameter.

Acknowledgement

This work was supported in part by the Chemicals and Metals Department, DOW Chemical, USA, by the Institute for Materials Science and Engineering of the Virginia Center for Innovative Technology, Grant No. MAT–86–028, and by the Office of Naval Research under Contract Number N00014–87–K–0042.

Notation

a	constant in Tafel line equation defined in Equation (3)
b	Tafel slope, V/decade
F	Faraday's constant, 96,487 C/equiv
I	total current, A
i	current density, A/m^2
i_{corr}	exchange current density of a freely corroding system, A/m^2
i_o	exchange current density, A/m^2
n	number of electrons transferred in reaction
R	gas constant, 8.314 J/K–mole
r	radial position, m
r_o	radius of a disk–electrode, m
SCE	Saturated Calomel Electrode
T	temperature, K
α	apparent transfer coefficient, dimensionless
β	apparent anodic or cathodic transfer coefficient (see also Equation (12))
δ	parameter defined in Equation (8)
η_c	concentration overpotential, V
η_s	surface overpotential, V
κ_∞	conductivity, mho/m
Φ_o	Ohmic potential drop, V
Φ	potential, V

Subscripts

a	anodic
app	applied
avg	average
c	cathodic
$corr$	corrosion
∞	bulk condition far from the electrode surface

References

1. M. M. Lowry, "Corrosion of Iron in Acidic Chloride Solutions," M.S. Thesis, University of Virginia, 1988.

2. M. M. Lowry, L. A. Joyce, O. C. Moghissi, C. B. Diem, and M. E. Orazem, "Corrosion of Iron in Acidic Chloride Solutions," in preparation, 1988.

3. J. Newman, "Resistance for Flow of Current to a Disk," *Journal of the Electrochemical Society*, **113** (1966), 501–502.

4. J. Newman, "Current Distribution on a Rotating Disk Below the Limiting Current," *Journal of the Electrochemical Society*, **113** (1966), 1235–1241.

5. J. Newman, *Electrochemical Systems*, Prentice-Hall, Inc., NJ, 1973.

6. C. Wagner and W. Traud, *Z. Electrochem.*, **44** (1938), 391ff.

7. M. Stern and A. L. Geary, "Electrochemical Polarization: I. A Theoretical Analysis of the Shape of Polarization Curves," *Journal of the Electrochemical Society*, **104** (1957), 56–63.

8. F. Mansfeld and K. B. Oldham, "A Modification of the Stern–Geary Linear Polarization Equation," *Corrosion Science* **11** (1971), 787–796.

9. F. Mansfeld, "Simultaneous Determination of Instantaneous Corrosion Rates and Tafel Slopes from Polarization Resistance Measurements," *Journal of the Electrochemical Society*, **120** (1973), 515–518.

10. F. Mansfeld, "Tafel Slopes and Corrosion Rates from Polarization Resistance Measurements," *Corrosion*, **29** (1973), 397–402.

11. F. Mansfeld, "Some Errors in Linear Polarization Measurements and Their Correction," *Corrosion*, **30** (1974), 92–96.

12. S. M. Gershakove, L. R. Udey, and F. Mansfeld, "An Improved Method for Analysis of Polarization Resistance Data," *Corrosion*, **37** (1981), 696–700.

13. S. Barnartt, "Two–point and Three–point Methods for the Investigation of Electrode Reaction Mechanisms," *Electrochimica Acta* **15** (1970), 1313–1324.

14. S. Barnartt, "Tafel Slopes for Iron Corrosion in Acidic Solutions," *Corrosion*, **27** (1971), 467–470.

15. B. D. McLaughlin, "A New Approach for Determining Corrosion Currents and Tafel Slopes," *Corrosion*, **37** (1981), 732–726.

16. J. Newman, "Ohmic Potential Measured by Interrupter Techniques," *Journal of the Electrochemical Society*, **117** (1970), 507–508.

17. K. Nisancioglu, "The Error in Polarization Resistance and Capacitance Measurements Resulting from Nonuniform Ohmic Potential Drop to Flush–Mounted Probes," *Corrosion* **43** (1987), 258–265.

18. S. Asakura and K. Nobe, "Electrodissolution Kinetics of Iron in Chloride Solutions. Part I. Neutral Solutions," *Journal of the Electrochemical Society*, **118** (1971), 13–18.

- C. B. Diem, B. Newman, and M. E. Orazem, "The Influence of Small Machining Errors on the Primary Current Distribution at a Recessed Electrode," *Journal of the Electrochemical Society*, in press.*

* The authors express their appreciation to Professor Eliezer Gileadi, Tel Aviv University, Israel, who suggested this problem. During the course of this work, B. Newman was supported by a fellowship from Texaco. This work was also supported in part by the Office of Naval Research under Contract Number N00014-87-K-0042. Computation costs for this work were provided through a grant from the University of Virginia Academic Computing Center.

The Influence of Small Machining Errors on the Primary Current Distribution at a Recessed Electrode*

Conrad B. Diem,† Bernard Newman, and Mark E. Orazem‡
Department of Chemical Engineering
University of Virginia
Charlottesville, Virginia 22901

June 1988

Abstract

The influence of small machining errors on the primary current distribution and resistance for a recessed electrode is explored though the use of conformal mapping coupled with numerical integration of the resulting integral equations. The influence of the depth to which the electrode is recessed and the angle between the electrode and the insulating wall is calculated for the current distribution on the electrode, the average current density that would be measured in an experimental cell, and the correction that would be made to compensate for cell resistance. The results show that the accuracy attainable in a modern machine shop is sufficient to justify neglecting the nonuniformity due to machining errors.

Key words: Cell Design, Potential

Introduction

Experimental systems for studying electrochemical reactions are often chosen such that the current distribution is uniform over the electrode surface. This simplifies comparison of experimental data to tractable mathematical models. The rotating disk, for example, is frequently used because the current distribution is uniform when the current is limited by transport of reacting species to the electrode. The current distribution below the mass–transfer–limited current, however, is not necessarily uniform, and the primary current distribution yields an infinite current density at the periphery of the disk.[1] Several systems can be chosen for which both the mass–transfer–limited and the primary current distribution are uniform. Concentric rotating cylinders are used for this application as are disk electrodes recessed in an insulating medium like epoxy or teflon.

---

* *Journal of the Electrochemical Society*, in press.

† student member

‡ member

The object of this work was to identify the effect of small machining errors on the uniformity of the current distribution on a recessed electrode. The specific topics addressed were:

- *The effect of small deviations from a right angle between the insulating wall and the recessed electrode.* The primary current density at the periphery of the electrode will be infinite for any interior angle greater than $\pi/2$, and will be equal to zero for any angle less than $\pi/2$. Since these changes in current density at the electrode edge take place for even small deviations from a right angle, our objective was to determine the extent to which unintentional deviations of the interior angle from $\pi/2$ could influence characteristics important to electrochemical experiments.
- *The effect of the depth to which the electrode is recessed.* This question has relevance to the fabrication of recessed electrodes (*i.e.,* how recessed should the electrode be to ensure a uniform distribution?).

A planar geometry was chosen for this study. The results presented here for the effect of the angle between the electrode and insulator and the electrode depth on current distribution apply approximately to a disk geometry because the curvature of the disk can be neglected in a region very close to the electrode periphery. The correction to quantities depending on integration over the electrode surface, such as the primary resistance and the average current densities, would be different for the two geometries.

Background

Primary current and potential distributions apply to systems for which the surface overpotential can be neglected and the phase adjacent to the electrode has a uniform potential. The primary distribution calculations presented here provide a guide based on a "worst–case" analysis because kinetic limitations, if present, would tend to make the current distribution be more uniform.[1] The primary distribution would be approached for large electrodes, large values of exchange current density or average current density, or for solutions of low conductivity (see, *e.g.,* reference (1)). Calculation of the primary current and potential distributions involves solution of Laplace's equation, $\nabla^2\Phi = 0$, which is not trivial, even for simple geometries. The method of images,[2] separation of variables,[3] and superposition[4,5] have been used to solve Laplace's equation for a number of systems. A review of analytic solutions has been presented by Fleck.[6]

The Schwarz–Christoffel transformation, a type of conformal mapping, provides a powerful tool for the solution of Laplace's equation in systems with planar boundaries. References (7-11) provide introductions to conformal mapping and to the Schwarz–Christoffel transformation. The application of the Schwarz–Christoffel transformation to obtain the primary resistance of a number of electrochemical cell geometries is given in references (12–14). This method was used by Moulton[15] to derive the current and potential distribution for two electrodes placed arbitrarily on the boundaries of a rectangle. Moulton's solution provides an asymptotic solution for the problem treated here in the limit that the depth to which the electrode is recessed approaches zero. Application of the Schwarz–Christoffel transformation is generally limited, however, by the difficulty of generating solutions to the

resulting integrals. Analytic solutions allow calculation of the primary current and potential distributions throughout the cell, but are possible for a limited number of system geometries. Numerical evaluation of these integrals allows calculation of both the primary current distribution along the electrodes and the cell resistance. This approach has been applied to the primary current distribution and resistance of cells with slotted electrodes,[16] and to the electrical resistance of compact tension specimens used in studies of fracture mechanics.[17]

Theoretical Development

The two–dimensional recessed electrode is shown schematically in Figure 1 where the heavy solid lines represent electrodes and the thin lines represent insulating surfaces. In treating its electrical characteristics, an insulating surface can replace the centerline which bisects this cell along a line perpendicular to the electrodes. Thus, the recessed electrode treated in this work is presented in Figure 2a where letters A through E represent the coordinates of corners in terms of the complex coordinate system

$$z = z_r + jz_j, \tag{1}$$

and O is the origin in this coordinate system. The Schwarz–Christoffel transformation maps a polygon in the z (complex) plane onto the t (complex) plane (see Figure 2b). The perimeter of the polygon is mapped onto the real axis, with the interior mapped onto the upper half–plane. The transformation to t–coordinates is given by

$$z = \int_0^t \frac{j(e-t)^{\beta/\pi}}{(-t)^{1/2}(a-t)^{1/2}(b-t)^{1/2}(c-t)^{1/2}(d-t)^{\beta/\pi}}dt, \tag{2}$$

where 0 and a through e represent the mapping of positions O and A through E onto the real t–axis. The Schwarz–Christoffel transformation can be applied a second time to map the t–coordinate positions onto the χ–plane shown in Figure 2c. Thus,

$$\chi = \int_0^t \frac{jdt}{(a-t)^{1/2}(b-t)^{1/2}(c-t)^{1/2}(d-t)^{1/2}}. \tag{3}$$

The solution to Laplace's equation for the rectangle in the χ–coordinate system (Figure 2c) is easily shown to be

$$\Phi = \frac{\chi_i}{\chi_{i,max}}V, \tag{4}$$

where $\chi_{i,max}$ is the distance between the two electrodes in Figure 2c, obtained by integrating equation (3) between the limits of c to d. The current density at the electrode in the χ–coordinate system is uniform and is proportional to the derivative of potential with respect to the imaginary component of χ, *i.e.*,

$$\left.\frac{\partial\Phi}{\partial\chi_i}\right|_{cd} = \frac{V}{\chi_{i,max}}. \tag{5}$$

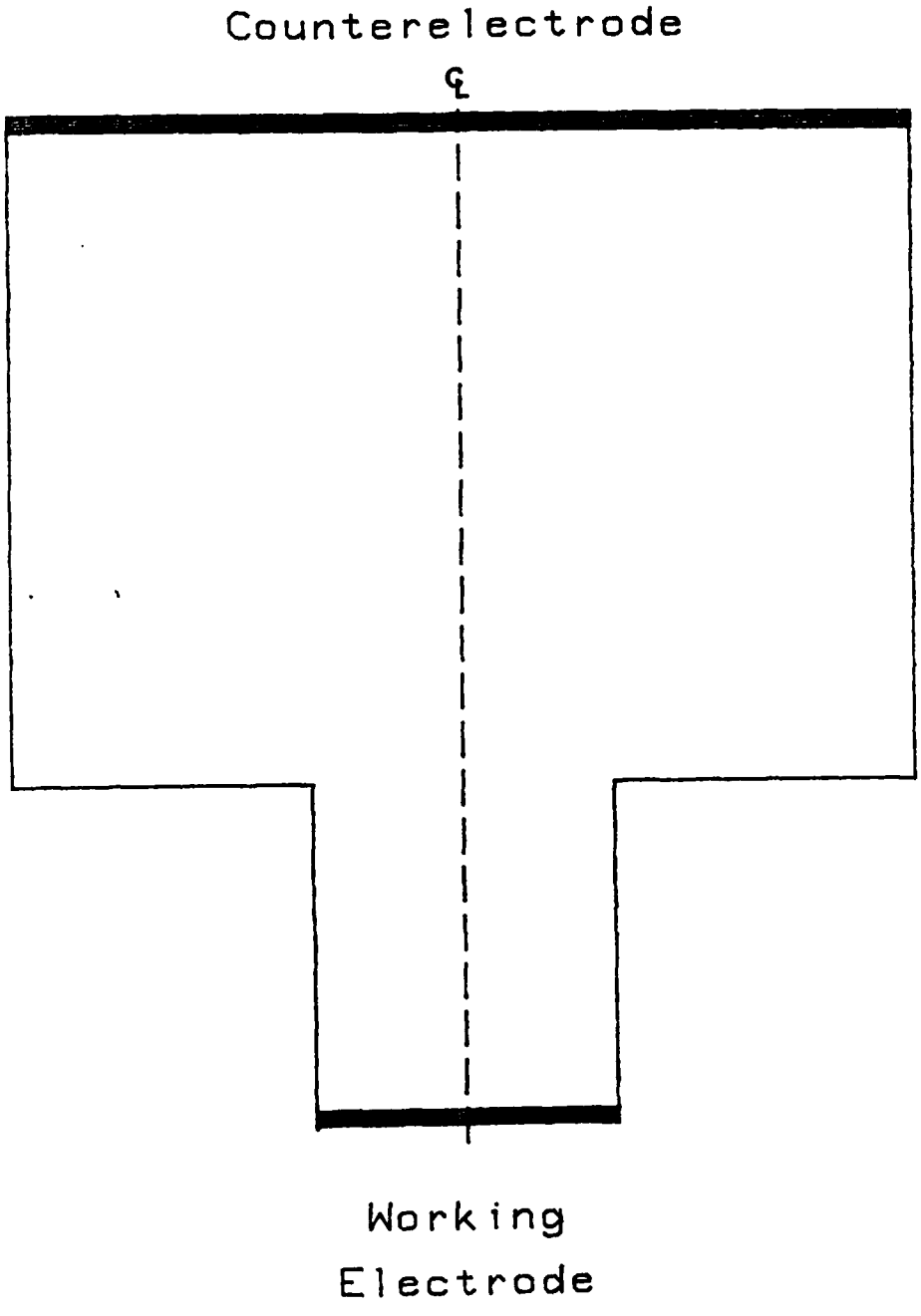

Figure 1. Schematic representation of the cell geometry.

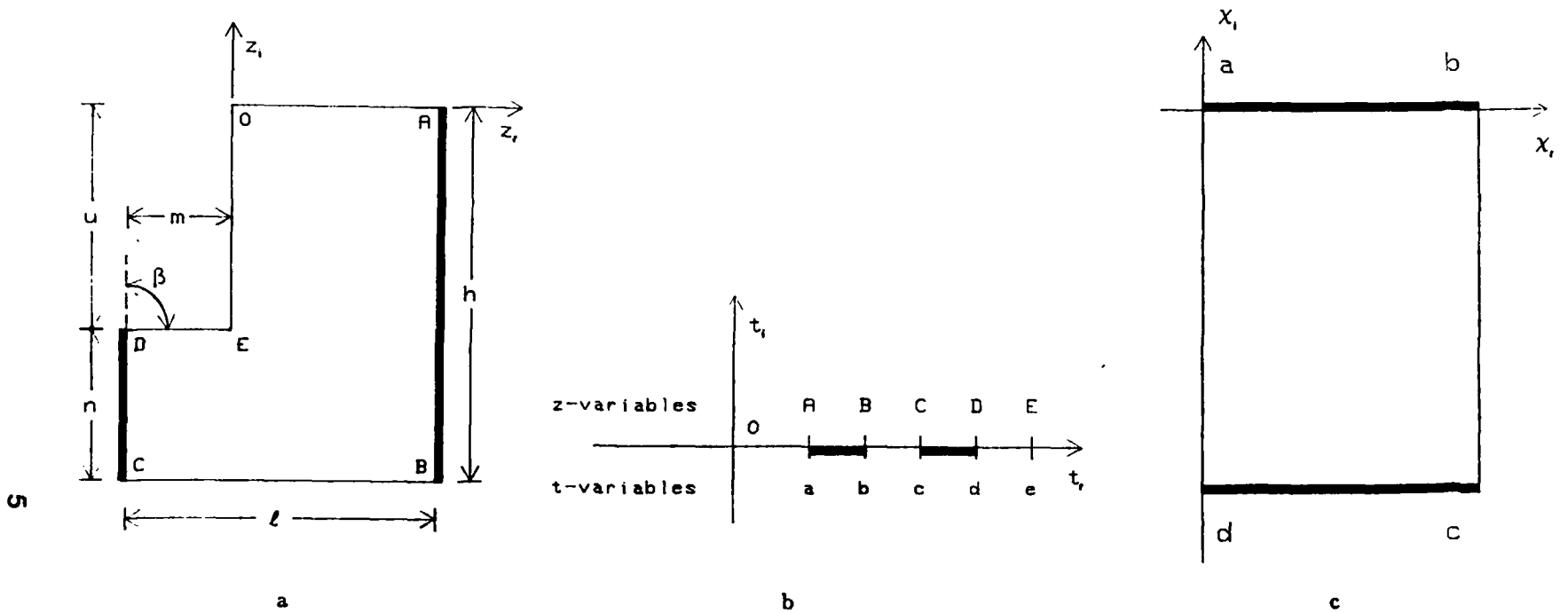

Figure 2. Schematic representation of the transformation of the cell geometry. a) $z = z_r + jz_j$; b) $t = t_r + jt_j$; and c) $\chi = \chi_r + j\chi_j$.

The derivative in equation (5) is related to the derivative of potential with respect to the imaginary component of t by

$$\left.\frac{\partial \Phi}{\partial \chi_i}\right|_{cd} = \left.\frac{\partial \Phi}{\partial t_i}\right|_{cd} \left.\frac{\partial t_i}{\partial \chi_i}\right|_{cd}, \tag{6}$$

or

$$\left.\frac{\partial \Phi}{\partial t_i}\right|_{cd} = j g(t_r) \left.\frac{\partial \Phi}{\partial \chi_i}\right|_{cd}, \tag{7}$$

where

$$g(t_r) = \frac{1}{(t-a)^{1/2}(t-b)^{1/2}(t-c)^{1/2}(d-t)^{1/2}}. \tag{8}$$

Equation (3) was used to obtain an expression for $\partial t_i / \partial \chi_i$ in terms of $g(t_r)$. The current density normal to the electrode in the original z–coordinate system is proportional to the derivative of potential with respect to the real component of z. Through use of equation (2), this derivative can be related by the chain rule to $\partial \Phi / \partial t_i$ and $\partial \Phi / \partial \chi_i$. Thus,

$$\left.\frac{\partial \Phi}{\partial z_r}\right|_{cd} = \left.\frac{\partial \Phi}{\partial t_i}\right|_{cd} \left.\frac{\partial t_i}{\partial z_r}\right|_{cd} \tag{9}$$

$$= \frac{g(t_r)}{f(t_r)} \left.\frac{\partial \Phi}{\partial \chi_i}\right|_{cd} \tag{10}$$

$$= \frac{g(t_r)}{f(t_r)} \frac{V}{\chi_{i,max}}, \tag{11}$$

where

$$f(t_r) = \frac{(e-t)^{\beta/\pi}}{t^{1/2}(t-a)^{1/2}(t-b)^{1/2}(t-c)^{1/2}(d-t)^{\beta/\pi}}. \tag{12}$$

Equations (8), (11), and (12) allow determination of the current density for the electrode cd and the electrical resistance for the cell. The current density is given by

$$i_{cd} = -\kappa \frac{\partial \Phi}{\partial z_r} = \frac{g(t_r)}{f(t_r)} \frac{\kappa V}{\chi_{i,max}}, \tag{13}$$

and the average current density is obtained by integrating over the electrode area, *i.e.*,

$$i_{avg} = \frac{-\int_C^D W \kappa \frac{\partial \Phi}{\partial z_r} dz}{W \int_C^D dz} \tag{14}$$

$$= \frac{-\int_C^D \frac{g(t_r)}{f(t_r)} \frac{\kappa V}{\chi_{i,max}} dz}{\int_C^D dz}. \tag{15}$$

The dimensionless primary resistance of the cell is given by

$$W \kappa R = \frac{j \chi_{i,max}}{\int_C^D \frac{-g(t_r)}{f(t_r)} dz}, \tag{16}$$

but, since $dz/dt = jf(t_r)$ along cd,

$$W\kappa R = \frac{\chi_{i,max}}{\int_c^d g(t_r)dt}. \tag{17}$$

Similarly,

$$\frac{i}{i_{avg}} = \frac{g(t_r)}{f(t_r)} \frac{D-C}{\int_c^d g(t_r)dt}. \tag{18}$$

The method presented above follows closely the development presented in references 16 and 17.

Numerical Method

The solution for this problem required finding the t–coordinates of the system corresponding to the positions A through E in the original (z) coordinate system. Five integral equations were obtained by setting the lengths of the five sides in z–coordinates equal to their transform from t–coordinates. The lengths were obtained from Figure 2a. The sixth side transforms to infinity and was not used. The equations solved were:

$$\ell - m = \int_0^a \frac{(e-t)^{\beta/\pi}}{t^{1/2}(a-t)^{1/2}(b-t)^{1/2}(c-t)^{1/2}(d-t)^{\beta/\pi}} dt, \tag{19}$$

$$-h = -\int_a^b \frac{(e-t)^{\beta/\pi}}{t^{1/2}(t-a)^{1/2}(b-t)^{1/2}(c-t)^{1/2}(d-t)^{\beta/\pi}} dt, \tag{20}$$

$$-\ell = -\int_b^c \frac{(e-t)^{\beta/\pi}}{t^{1/2}(t-a)^{1/2}(t-b)^{1/2}(c-t)^{1/2}(d-t)^{\beta/\pi}} dt, \tag{21}$$

$$h - u = \int_c^d \frac{(e-t)^{\beta/\pi}}{t^{1/2}(t-a)^{1/2}(t-b)^{1/2}(t-c)^{1/2}(d-t)^{\beta/\pi}} dt, \tag{22}$$

and

$$m\sqrt{1+\tan^2(\pi/2-\beta)} = \int_d^e \frac{(e-t)^{\beta/\pi}}{t^{1/2}(t-a)^{1/2}(t-b)^{1/2}(t-c)^{1/2}(t-d)^{\beta/\pi}} dt. \tag{23}$$

The solution to these integral equations was iterative:

1. a, b, c, d,and e were guessed.
2. The integrals were calculated numerically, and a vector $\vec{G}_i(\vec{x})$ was calculated, where $\vec{G}_i$ is the five element vector composed of the closure error of the five equations above and $\vec{x}$ is the vector of guesses for a, b, c, d, and e.
3. Convergence was obtained by a method similar to the Newton–Raphson method. A matrix of partial derivatives

$$B_{ik} = \frac{\partial \vec{G}_i}{\partial \vec{x}_k} \tag{24}$$

were calculated using a forward–difference formula, and a correction vector was calculated as

$$-\vec{G}_i = B_{ik}\,\Delta\vec{x}. \tag{25}$$

The convergence condition for this set of equations was $\vec{G}(\vec{x}) = 0$ (or $\Delta\vec{x} = 0$). Convergence was very sensitive to the initial guesses for a through e, and a predictor–corrector method (see References (17) and (18)) was used to reduce computer time.

Several additional tricks were necessary to complete this solution. It is impossible, of course, to integrate directly on a section where the integrand is singular. This problem was solved by making a variable substitution and by restricting the number of singularities for each integral to one by dividing each interval in half. For example, an integral of the form

$$\int_c^d \frac{dt}{f(t)(t-c)^{1/\alpha}(d-t)^{1/\beta}},$$

was split into two terms that each contain only one singularity, *i.e.*,

$$\int_c^{(c+d)/2} \frac{dt}{f(t)(t-c)^{1/\alpha}(d-t)^{1/\beta}} + \int_{(c+d)/2}^d \frac{dt}{f(t)(t-c)^{1/\alpha}(d-t)^{1/\beta}}.$$

The variable substitution

$$u = (t-c)^{1-1/\alpha} \tag{26}$$

or

$$t = c + u^{1/(1-1/\alpha)} \tag{27}$$

was used to obtain a nonsingular expression for the first integral, *i.e.*,

$$\frac{1}{1-1/\alpha}\int_c^{(c+d)/2} \frac{du}{f(t)(d-t)^{1/\beta}}.$$

The expression for t in equation (27) is substituted before integrating by Simpson's rule. The number of divisions of the integration interval was doubled until successive calculations of an integral agreed to at least six significant figures. The convergence criterion used for step 3 was that successive calculations of a through e agree within five significant figures.

Results and Discussion

The primary current distribution and resistance are determined by the angle β/π and by the geometric ratios h/k, n/h, and m/n. The effect of the cell geometry outside the recessed electrode, *i.e.*, the rectangle formed by allowing the depth m to be equal to zero, was treated by Moulton.[15] Therefore, the values for $h/(\ell - m)$ and n/h were held fixed at 1.622 and 0.2, respectively. The parameters chosen for study here were those directly associated with the recessed electrode: the angle β and the aspect ratio m/n. The questions of primary interest to the experimentalist would be how deep the recessed electrode should be to have a uniform primary current distribution, and how much effect an unintentional deviation from a right angle between the electrode and insulating wall would have on the current distribution, the average current density, and the resistance of the cell.

Current Distribution for an Isolated Electrode

The qualitative behavior of the primary current distribution for plane electrodes is based on the solution of Laplace's equation for an isolated plane electrode intersected by an insulator at an angle β (see Figure 3). The behavior of the current density in the region close to the intersection of the two planes is given by

$$i(x) \propto \left(\frac{n-x}{n}\right)^{-\frac{1/2-\beta/\pi}{1-\beta/\pi}}, \tag{28}$$

where $n-x$ is the distance from the intersection point. For $\beta = \pi/2$ the current density approaches a finite value at $x = n$. For $\beta > \pi/2$ the current density is zero at $x = n$, while for $\beta < \pi/2$ the current density is infinite at $x = n$. This limiting case shows that even small changes in the angle β about $\pi/2$ can lead to large changes in the current density very close to the insulating wall. Equation (28) also provides an asymptotic limit whereby the numerical results can be compared.

Current Distribution for a Recessed Electrode

The effect of aspect ratio m/n on the current distribution is presented in Figure 4. The limit as m/n approaches zero is given by Moulton and shows an infinite current at the electrode periphery. The current distribution becomes uniform as m/n becomes large. The current density at the central portion of the recessed electrode ($x = 0$) provides an indication of the uniformity of the current distribution and is presented in Figure 5 as a function of m/n. An aspect ratio of $m/n = 2$ is sufficient to cause the primary distribution to be uniform. The calculations do not treat the effect of mass–transfer and kinetic limitations to electrochemical reactions. Kinetic limitations would tend to make the (secondary) current distribution more uniform at aspect ratios less than 2.[1]

While these calculations were for a planar geometry, the results presented here apply approximately to a disk geometry because the curvature of the disk can be neglected in a region very close to the electrode periphery. Quantities that depend upon integration over the electrode surface would, of course, be different for the two geometries. For example, the current density at the center of a non–recessed electrode (see $m/n = 0$ in Figure 5) is equal to 0.68 when normalized by the average current density obtained by integration of the corresponding current distribution over a planar surface. When this current distribution is averaged over a circular surface with n replaced by the disk radius, the normalized current density is equal to 0.5 which is the value expected for a disk electrode. Figure 5 can be used to estimate the depth to which an electrode should be recessed to provide a uniform current distribution for both planar or disk geometries because, for either case, the current at the center of the electrode approaches the average current density for large values of m/n. The value of the normalized current at the center of the electrode would be different for the two geometries when m/n becomes small.

The current distribution that results from changing the angle β/π is also a function of the depth m/n. The effect of small changes in angle is presented in Figures 6 and 7 for

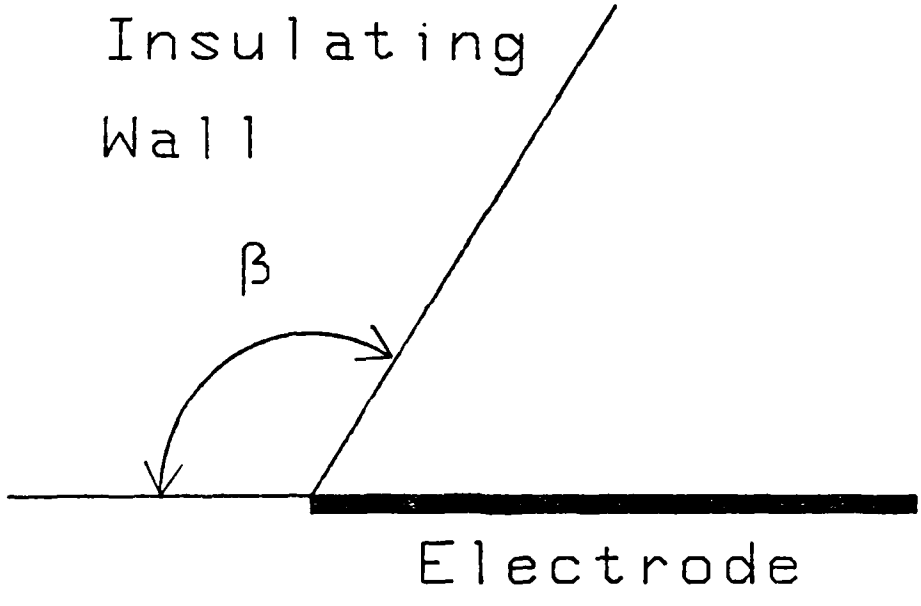

Figure 3. Schematic representation of an isolated electrode.

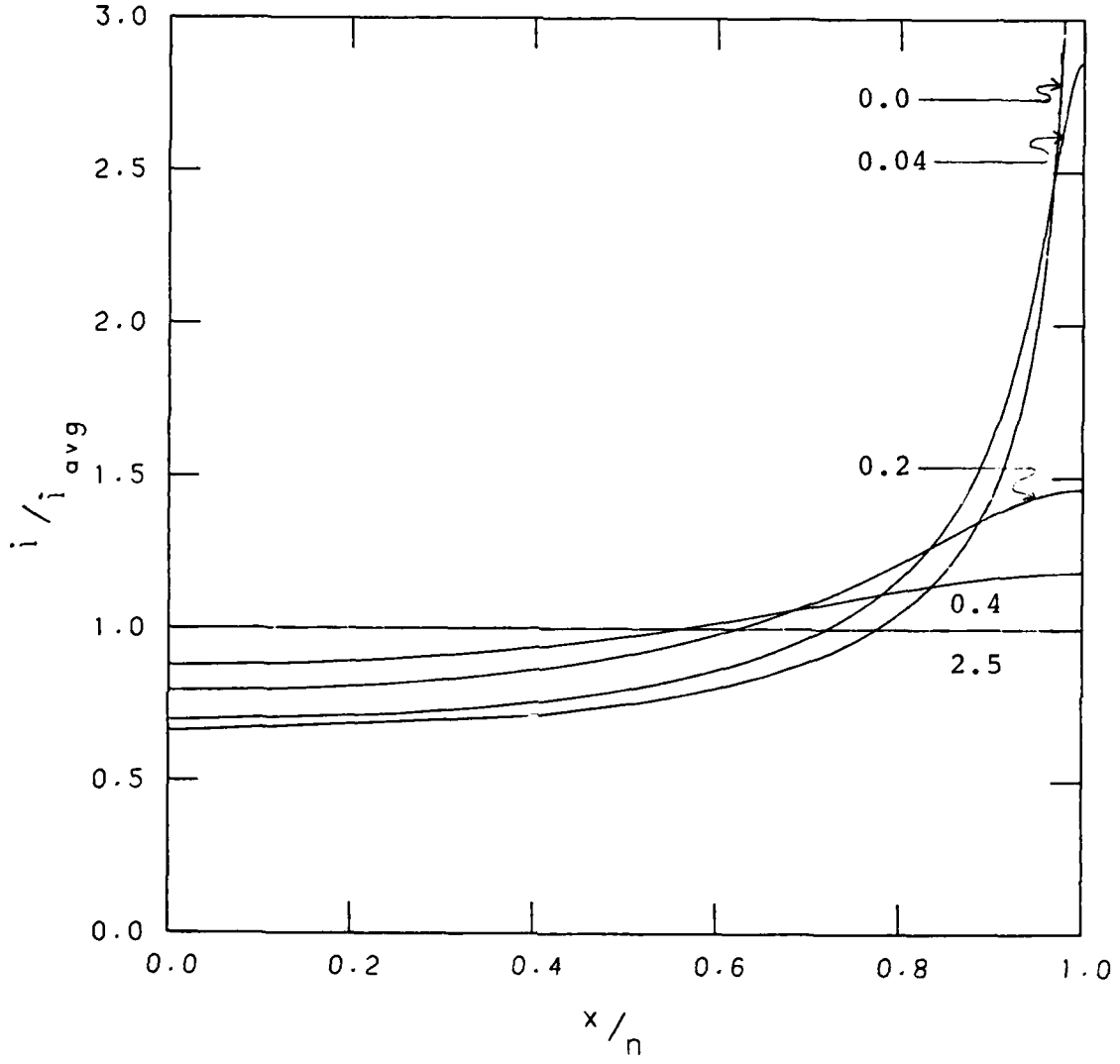

Figure 4. Current distribution with the aspect ratio m/n as a parameter for $\beta/\pi = 0.5$.

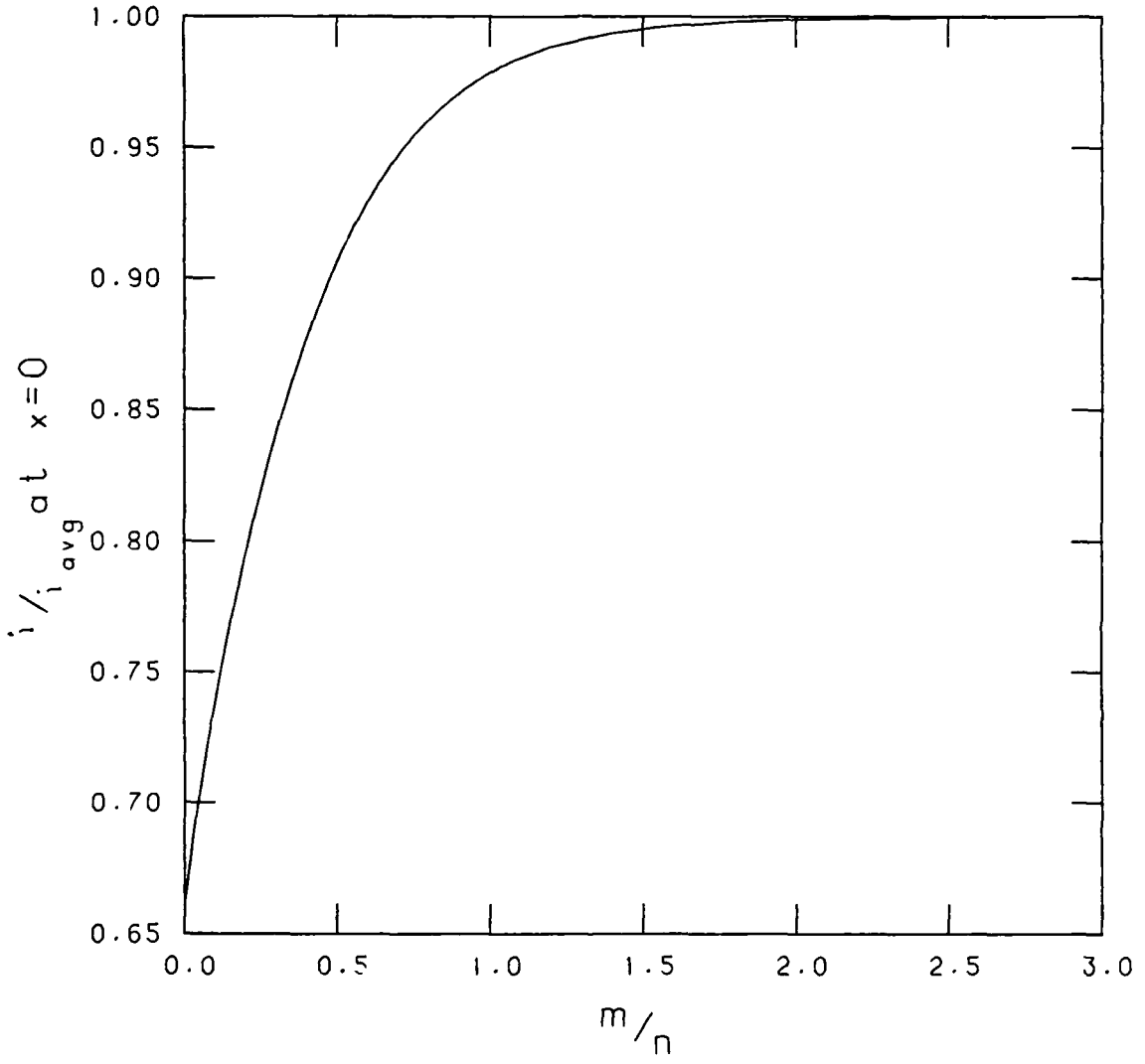

Figure 5. The current density at the center of the recessed electrode as a function of the aspect ratio m/n for $\beta/\pi = 0.5$.

the current distribution on deep and shallow electrodes, respectively. The variation in β studied here corresponds to ± 1.8 degrees from a right angle. The current density is uniform for $\beta/\pi = 0.5$. The current at the periphery is equal to zero for $\beta/\pi > 0.5$ and tends to infinity according to equation (28) for $\beta/\pi < 0.5$. The current density at the center of the electrode is presented in Figure 8 as a function of β/π for both the deep and the shallow electrodes. The ratio of the current density at $x = 0$ to the average current density is equal to one for a deep electrode with an angle of $\pi/2$ ($\beta/\pi = 0.5$). For a shallow electrode, this ratio tends toward one only for values of β/π greater than 0.5. This result is seen because the nonuniformity associated with a small aspect ratio m/n can be canceled in part by the nonuniformity associated with $\beta/\pi > 0.5$.

Average Current Density for a Recessed Electrode

As seen in the preceding section, the geometry of the recessed electrode has a significant impact on the current distribution. An interior angle greater than $\pi/2$ ($\beta/\pi < 0.5$) causes the current distribution to be infinite at the periphery of the electrode and causes the average current density to be larger than it would be for a perfect right angle. The percent error in the average current density relative to $\beta/\pi = 0.5$, defined to be

$$\epsilon(\beta/\pi) = \frac{i_{avg}(\beta/\pi) - i_{avg}(\beta/\pi = 0.5)}{i_{avg}(\beta/\pi = 0.5)} \times 100\%, \tag{29}$$

is presented in Figure 9 as a function of β/π with m/n as a parameter. This error is a function of the depth to which the electrode is recessed because, for a fixed value of β/π, the displacement of electrolyte is larger for a deeper electrode. For an electrode sufficiently deep that the current distribution for a perfect right angle between electrode and insulator may be regarded to be uniform, the average current density measured would be 4 percent higher for a 1.8 degree deviation from a right angle (corresponding to $\beta/\pi = 0.49$) than it would be for the ideal right–angle geometry.

Primary Resistance for a Recessed Electrode

The major interest to the experimentalist of the effect of the recessed electrode geometry on the primary resistance, presented below, would be in estimating *a priori* the cell resistance. It is not used here as a criterion for specification of tolerances because independent measurement of this resistance can be made by current interruption.

The primary resistance of the cell can be expressed in terms of the dimensionless group $W\kappa R$, where W is the cell width in the dimension coming out of the plane of Figure 2a. In the limit that the aspect ratio m/n approaches zero, the primary resistance approaches that of a rectangle of length h and width k and with electrodes of width h and n. The solution for this problem has been presented by Moulton[15] in terms of tabulated elliptic functions[19] as

$$W\kappa R_m = \frac{K(1 - m_\lambda)}{K(m_\lambda)} \tag{30}$$

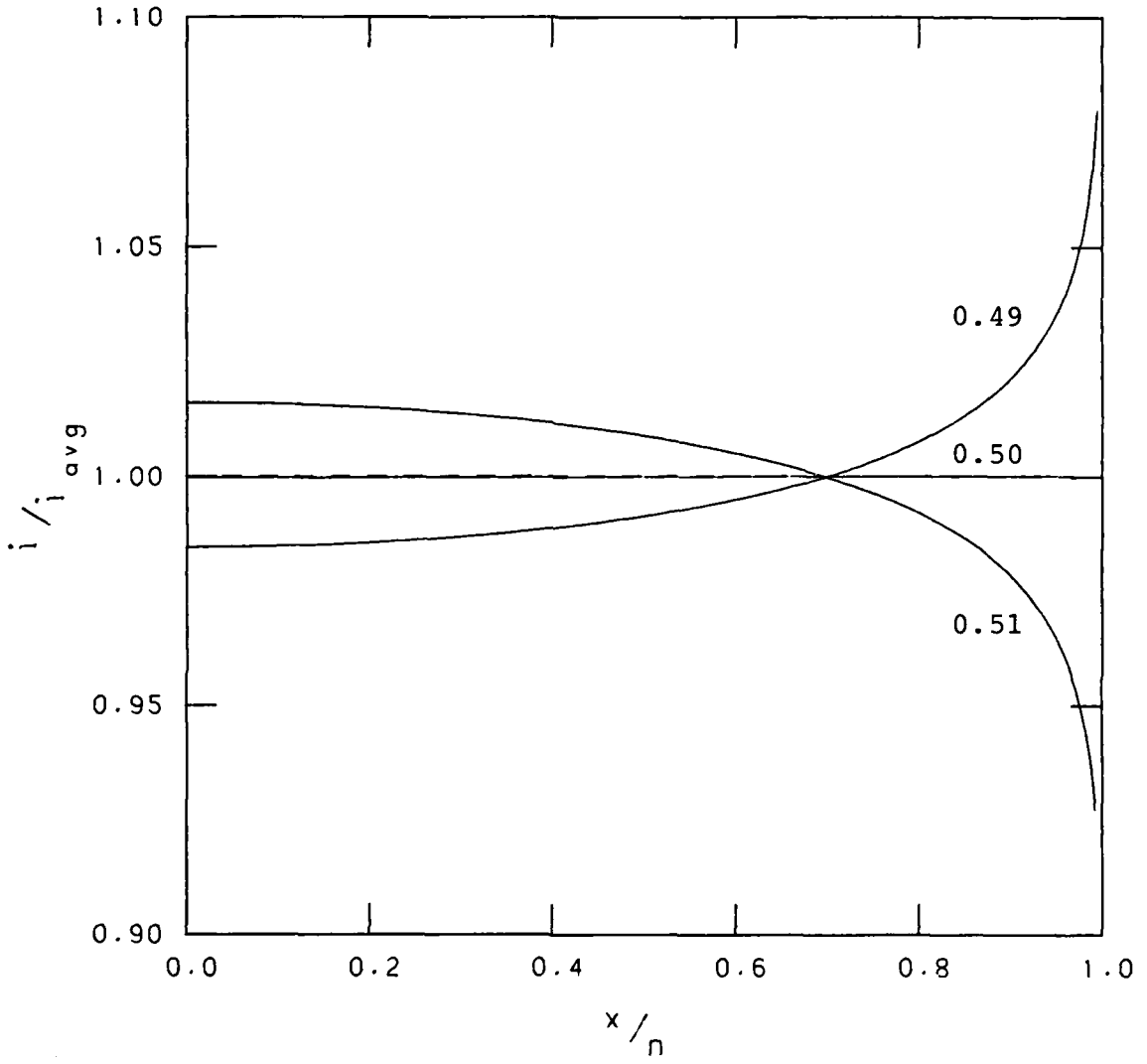

Figure 6. Current distribution with the angle β/π as a parameter for a deep electrode (aspect ratio $m/n = 2.52$).

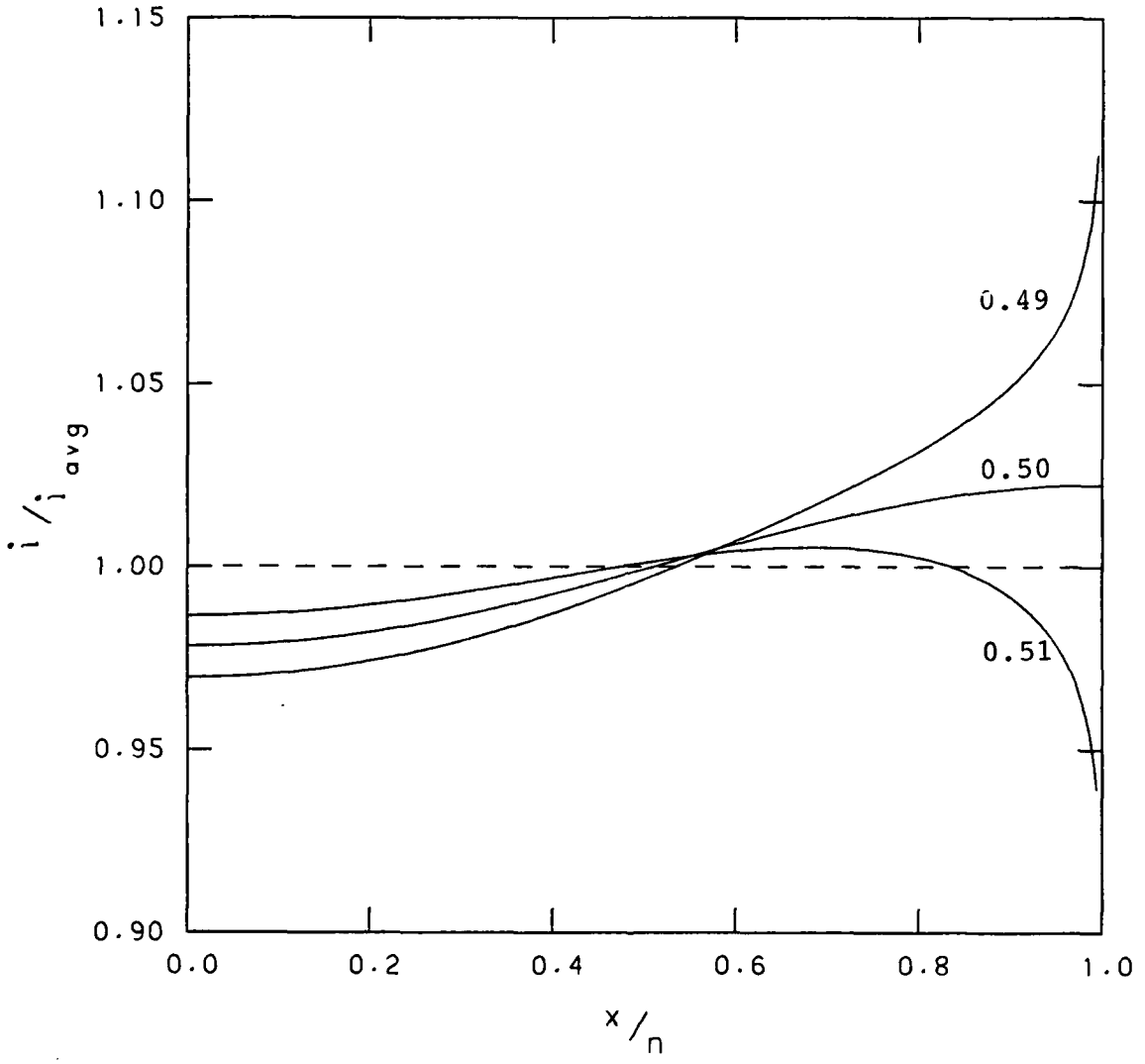

Figure 7. Current distribution with the angle β/π as a parameter for a shallow electrode (aspect ratio $m/n = 1.0$).

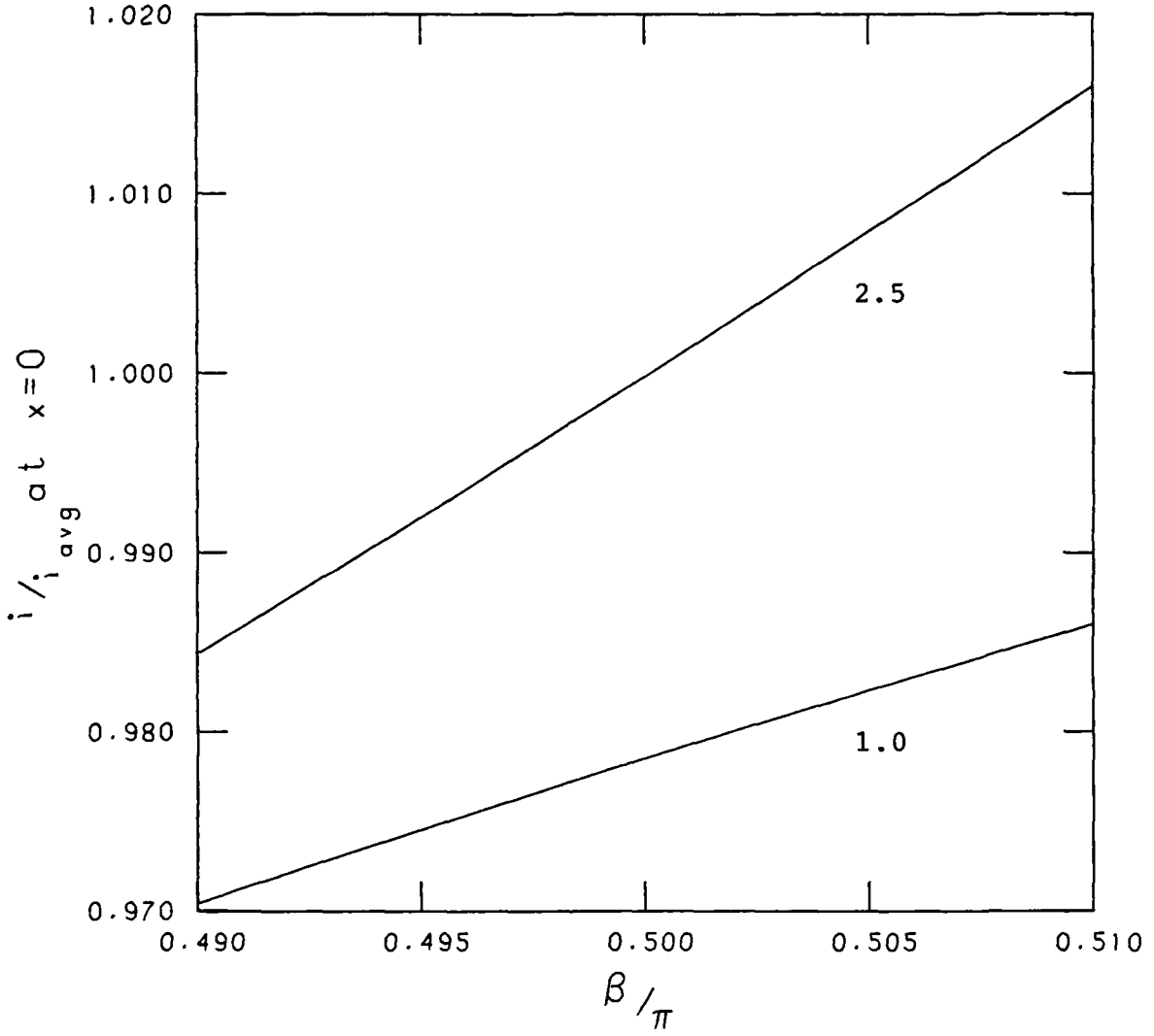

Figure 8. The current density at the center of the recessed electrode as a function of β/π with the aspect ratio m/n as a parameter.

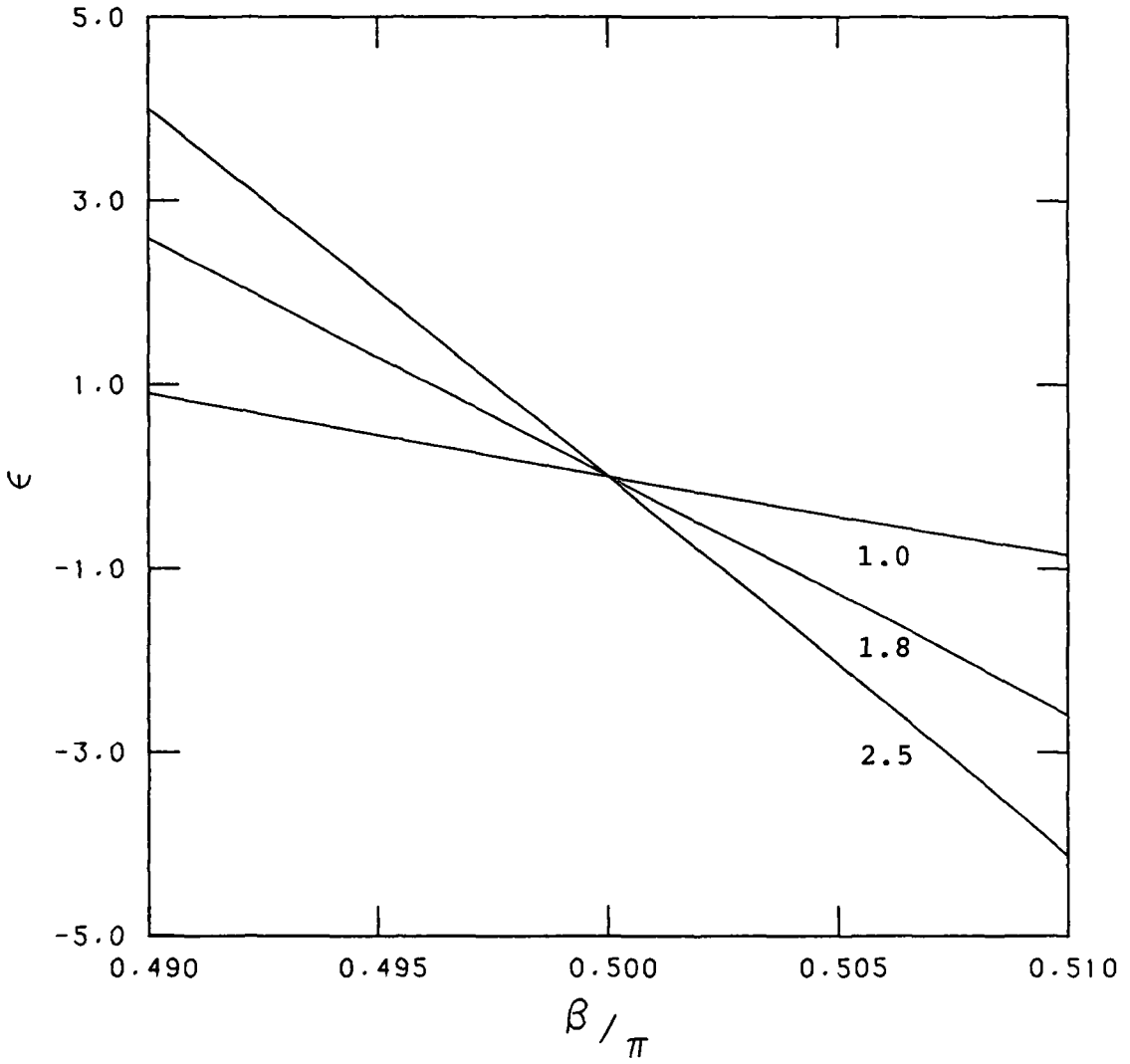

Figure 9. The percent error in the average current density relative to $\beta/\pi = 0.5$ as a function of β/π with m/n as a parameter.

where $K(m_\lambda)$ is the complete elliptic integral of the first kind with parameter m_λ. The parameter m_λ is obtained from the geometry of the rectangle by

$$m_\lambda = \frac{\mathrm{sn}^2(z_2|m) - \mathrm{sn}^2(z_1|m)}{\mathrm{sn}^2(z_3|m) - \mathrm{sn}^2(z_1|m)} \tag{31}$$

where m is the parameter defined by $K(1-m)/K(m) = k/h$, z_1 is the location of point B, z_2 is the location of point A, and z_3 is the location of point D. Equation (16.23.1) in reference (19) was used to calculate values for the elliptic function "sn".

The resistance can be approximated by the sum of the resistance associated with the rectangle $k\bar{h}$ and the rectangle $\bar{m}n$. Thus,

$$W\kappa R = W\kappa R_m + m/n + \Delta_1, \tag{32}$$

where Δ_1 is the correction that accounts for the constriction of current lines in the mouth of the recessed portion of the cell. The correction Δ_1 is presented in Figure 10 as a function of the aspect ratio m/n. The correction is equal to zero for $m = 0$ and approaches a constant value of 0.0367 as m/n becomes large. Δ_1, however, becomes a smaller fraction of the total dimensionless resistance $W\kappa R$ at large values of m/n because the resistance is proportional to m/n. The presentation of Δ_1 (as opposed to a presentation of the percent error in neglecting this term in equation (32)) allows a more general application of these results because Moulton's solution $W\kappa R_m$ accounts for the influence of the counterelectrode size and placement and for the size of the cell outside the recessed portion, and the term m/n accounts for the depth and width of the recessed electrode. The percent error is a function of geometric factors that are independent of the geometry of the recessed electrode. For the geometry treated here, $W\kappa R_m$ is equal to 1.195. The error in neglecting Δ_1 for a deep electrode (with m/n greater than 2.5) is less than one percent.

The angle β/π also has an effect on the primary resistance, even for very small deviations from 0.5, and the magnitude of Δ_1 is a function of the electrode depth. The effect of angle on Δ_1 is shown in Figure 11 with the aspect ratio m/n as a parameter. For m/n greater than one, all curves in Figure 11 yield a value of 0.0367 for Δ_1 at $\beta/\pi = 0.5$. Δ_1 reaches a value of 0.15 for a deep electrode ($m/n = 2.5$) with $\beta/\pi = 0.51$. The percent error caused by neglecting this term can, however, be reduced by a slight modification of equation (32), as shown below.

In calculating Δ_1 (equation (32)), the primary resistance associated with the exterior part of the cell was calculated using an electrode width of $n - m\tan(\beta - \pi/2)$, and the resistance associated with the recessed electrode was given by m/n. The influence of the parameter β/π could be reduced by replacing m/n in equation (32) with the arithmetic average of the resistance for a rectangle with electrode width n (*i.e.*, m/n) and the resistance for a rectangle with electrode width $n - m\tan(\beta - \pi/2)$ (*i.e.*, $m/(n - m\tan(\beta - \pi/2))$). Thus,

$$W\kappa R = W\kappa R_m + \frac{m}{n}\frac{2n - m\tan(\beta - \pi/2)}{2(n - m\tan(\beta - \pi/2))} + \Delta_2. \tag{33}$$

The correction to equation (33) Δ_2 is presented in Figure 12 as a function of β/π with m/n as a parameter. For $\beta/\pi = 0.5$, Δ_2 is equal to Δ_1 and is equal to 0.0367 for m/n greater than one. For a deep electrode, the error in assuming that Δ_2 is equal to 0.0367 is about 0.2 percent, and the error in neglecting Δ_2 altogether in equation (33) is less than two percent. In contrast, the error in neglecting Δ_1 in equation (32) for $\beta/\pi = 0.51$ (see Figure 11) is almost five percent.

Conclusions

The conformal mapping technique is ideally suited to determine the influence of small changes in the angle between the electrode and insulator on the primary current distribution for recessed electrodes. It is difficult to use finite–element or finite–difference techniques to obtain accurate values for current density near singular regions, such as seen at the electrode edge for $\beta/\pi < 0.5$. These numerical methods work well and, indeed, are necessary in the more common cases where kinetic limitations eliminate the singularities.

The results presented here show that the primary resistance does not undergo discontinuous behavior as the angle in the pit changes and that it can be approximated to be the sum of Moulton's solution for the influence of the geometry of the main portion of the cell and a term which treats the influence of the depth of the recessed portion of the cell. For a deep electrode, this expression is accurate to within one percent.

The approach to a uniform current distribution with increasing depth and variations in average current density with angle were used as criteria to identify specifications for a recessed electrode. The results presented here show that a recessed electrode with an aspect ratio of about 2.5 (calculated for the electrode half–width) is sufficiently deep to give a uniform current distribution. The average current is the quantity that would usually be obtained in an experiment by dividing the measured total current by the electrode area. For an electrode of this depth, a deviation of the angle between the electrode and the insulating wall by 0.5 degrees from a right angle ($|\beta/\pi - 0.5| = 0.0028$) causes the average current to deviate from the value expected for a perfect right angle by about 1.2 percent. These results suggest that specification of the angle between recessed electrode and insulating wall to within ± 0.5 degrees (a level of precision that can be routinely achieved in our machine shop) is sufficient to avoid significant errors in the measured current. The results presented here provide a guide based on a "worst–case" analysis because kinetic limitations, if present, would tend to make the current distribution be more uniform.

Acknowledgement

The authors express their appreciation to Professor Eliezer Gileadi, Tel Aviv University, Israel, who suggested this problem. During the course of this work, B. Newman was supported by a fellowship from Texaco. This work was also supported in part by the Office of Naval Research under Contract Number N00014–87–K–0042. Computation costs for this work were provided through a grant from the University of Virginia Academic Computing Center.

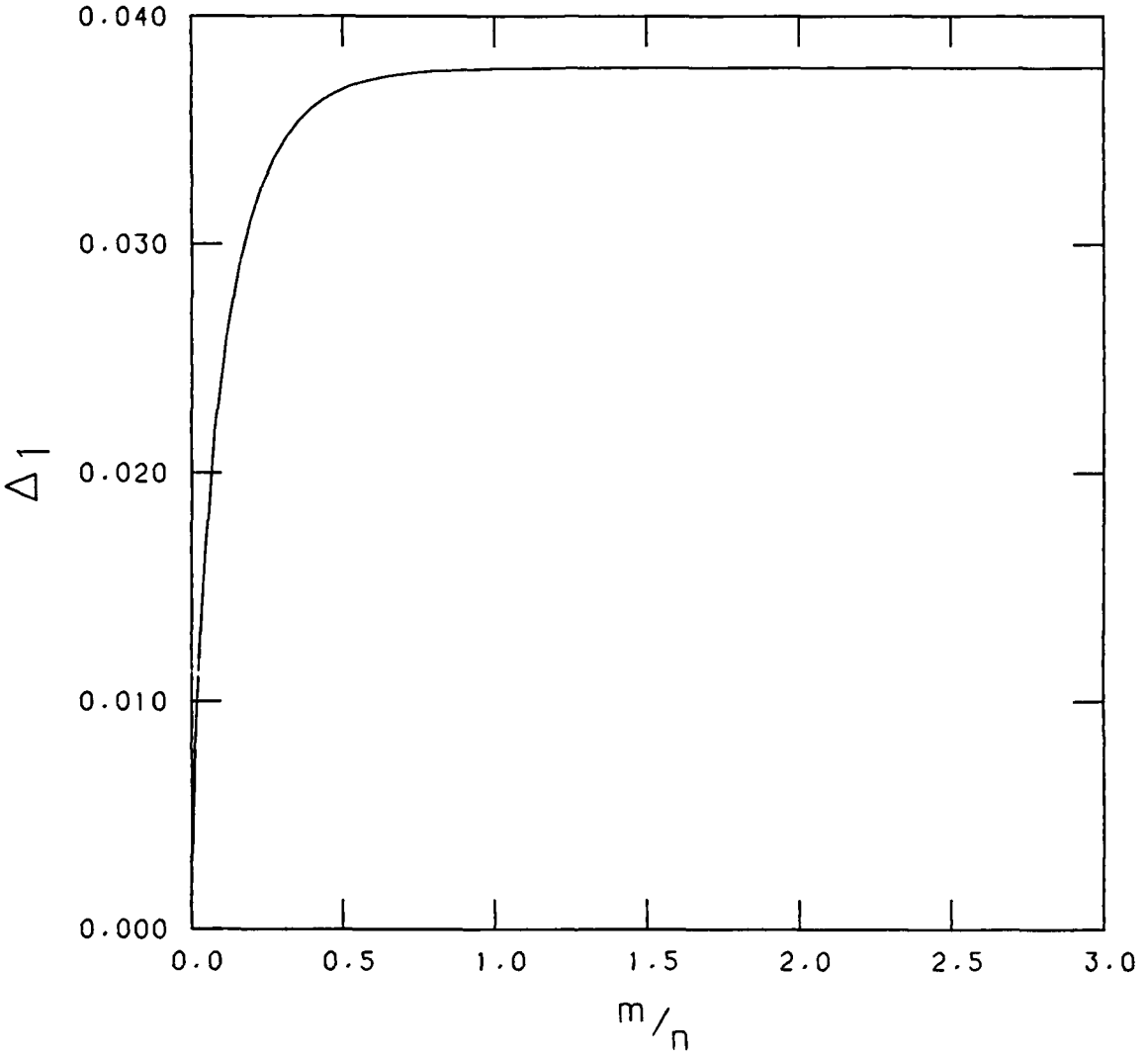

Figure 10. Correction to the primary resistance as a function of the aspect ratio m/n for $\beta/\pi = 0.5$.

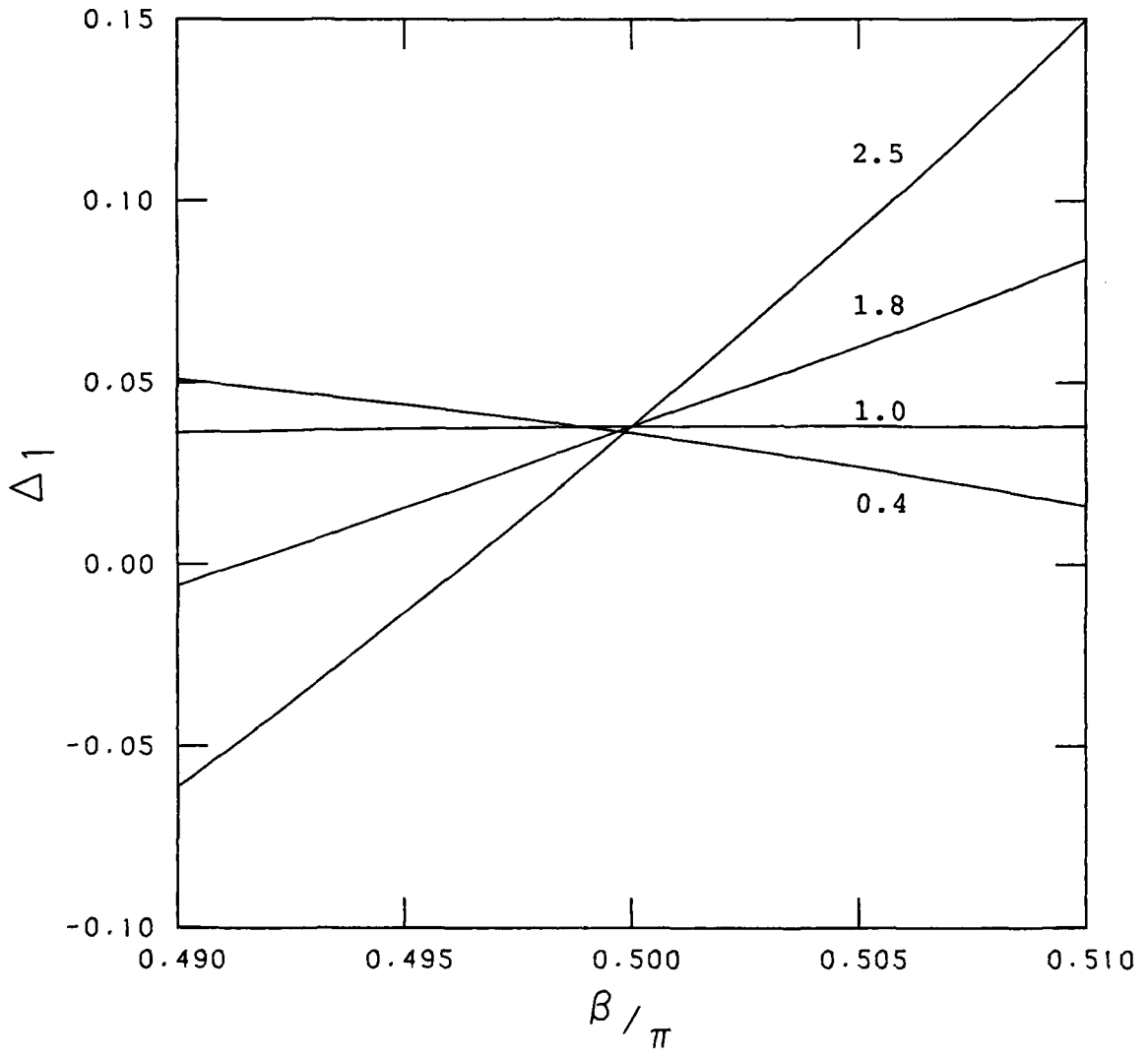

Figure 11. Correction to the primary resistance Δ_1 as a function of the angle β/π with aspect ratio m/n as a parameter.

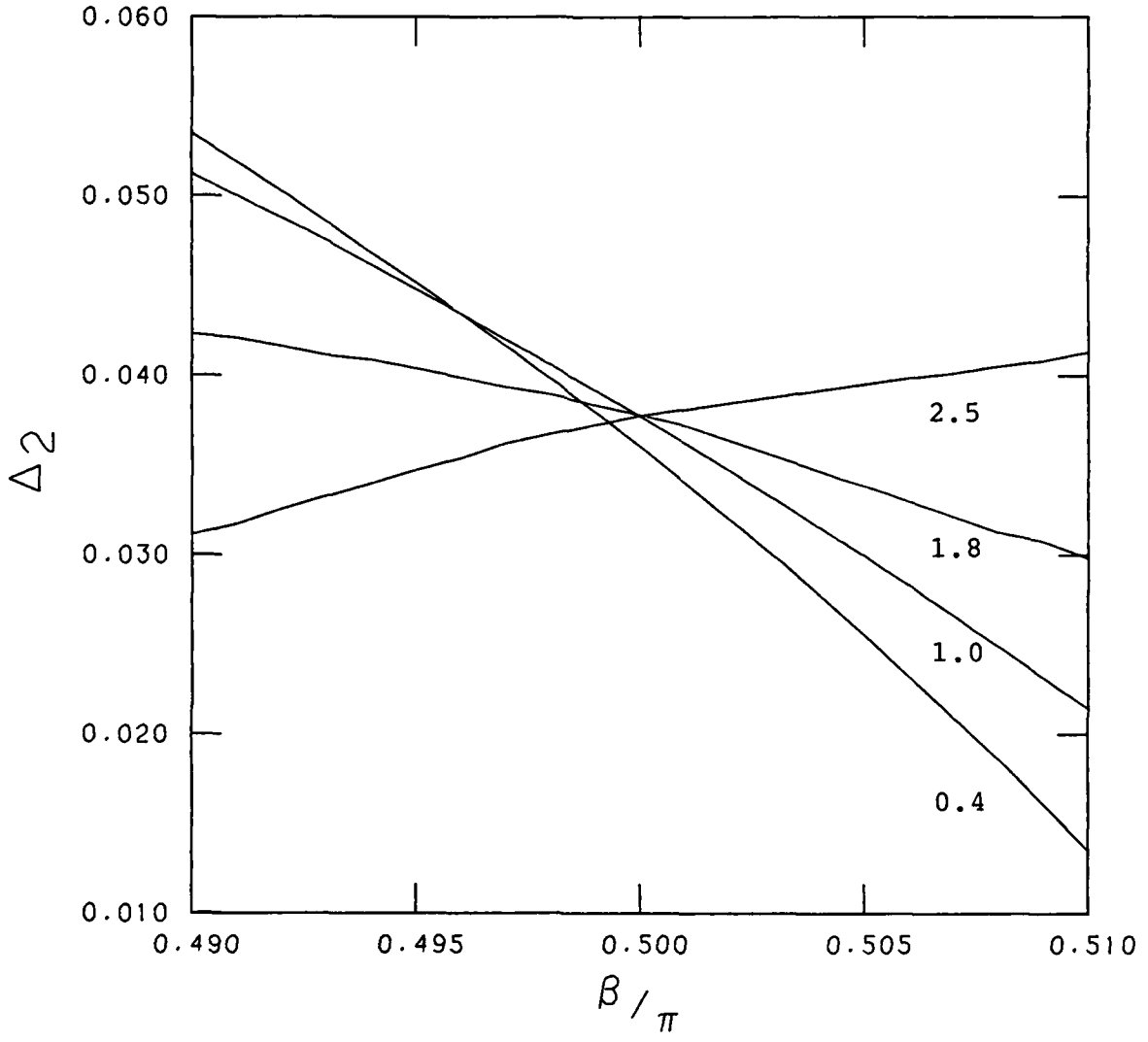

Figure 12. Correction to the primary resistance Δ_2 as a function of the angle β/π with aspect ratio m/n as a parameter.

Notation

Roman Characters

- a location of a corner in the t–coordinate system (see Figure 2b)
- A location of a corner in the original z–coordinate system (see Figure 2a)
- b location of a corner in the t–coordinate system (see Figure 2b)
- B location of a corner in the original z–coordinate system (see Figure 2a)
- c location of a corner in the t–coordinate system (see Figure 2b)
- C location of a corner in the original z–coordinate system (see Figure 2a)
- d location of a corner in the t–coordinate system (see Figure 2b)
- D location of a corner in the original z–coordinate system (see Figure 2a)
- e location of a corner in the t–coordinate system (see Figure 2b)
- E location of a corner in the original z–coordinate system (see Figure 2a)
- h the width of the counterelectrode (see Figure 2a)
- i current density, $\mathrm{mA/cm^2}$
- j the imaginary number, $\sqrt{-1}$
- ℓ the distance between working and counterelectrode (see Figure 2a)
- m the depth of the recess for the working electrode (see Figure 2a)
- n the half–width of the working electrode (see Figure 2a)
- R half–cell resistance, ohms
- t coordinate system for the intermediate half plane (see Figure 2b)
- u $h - n$ (see Figure 2a)
- V cell potential, V
- W cell thickness, cm (see Figure 2a)
- z original coordinate system (see Figure 2a)

Greek Characters

- β exterior angle between the recessed electrode and the insulating wall (see Figure 2a)
- Δ_1 error term in equation (32)
- Δ_2 error term in equation (33)
- ϵ percent error in average current density relative to $\beta/\pi = 0.5$, defined in equation (29)
- κ conductivity, mho/cm
- Φ electrical potential, V
- χ coordinate system for the rectangular geometry for which Laplace's equation can be easily solved (see Figure 2c)

Subscripts

avg	average
i	imaginary component
r	real component

References

1. Newman, John, "Current Distribution on a Rotating Disk Below the Limiting Current," *Journal of the Electrochemical Society* **113** (1966), 1235–1241.
2. Kasper, Charles, "The Theory of the Potential and the Technical Practice of Electrodeposition," *Transactions of the Electrochemical Society* **77** (1940), 353–384; **78** (1940), 131–160; **82** (1942), 153–184.
3. Newman, John, "Resistance for Flow of Current to a Disk," *Journal of the Electrochemical Society* **113** (1966), 501–502.
4. Miksis, Joseph J., Jr., and John Newman, "Primary Resistances for Ring–Disk Electrodes," *Journal of the Electrochemical Society* **123** (1976), 1030–1036.
5. Pierini, Peter, and John Newman, "Potential Distribution for Disk Electrodes in Axisymmetric Cylindrical Cells," *Journal of the Electrochemical Society* **126** (1979), 1348–1352.
6. Fleck, R. N., *Numerical Evaluation of Current Distribution in Electrochemical Systems*, M. S. thesis, University of California, Berkeley, September, 1964 (UCRL–11612).
7. Copson, E. T., *An Introduction to the Theory of Functions of a Complex Variable*, Oxford University Press, London, 1935.
8. Bowman, F., *Introduction to Elliptic Functions with Applications*, John Wiley and Sons, New York, 1953.
9. Churchill, Ruel V., *Complex Variables and Applications*, second edition, McGraw–Hill Book Company, New York, 1960.
10. Boas, M.L. *Mathematical Methods in the Physical Sciences*, John Wiley and Sons, New York, 1969.
11. Hauser, A.A. *Complex Variables with Physical Applications*, Simon and Schuster, New York, 1971.
12. Hine, Fumio, Shiro Yoshizawa, and Shinzo Okada, "Effect of the Walls of Electrolytic Cells on Current Distribution," *Journal of the Electrochemical Society* **103** (1956), 186–193.
13. Wagner, Carl, "Calculation of the Current Distribution at Electrodes involving Slots," *Plating* **48** (1961), 997–1002.
14. Newman, John, "The Fundamental Principles of Current Distribution in Electrochemical Cells," in *Electroanalytical Chemistry*, A. J. Bard, editor, volume 6 (1973), 187–352.
15. Moulton, H. Fletcher, "Current Flow in Rectangular Conductors," *Proceedings of the London Mathematical Society (Ser. 2)* **3** (1905), 104–110.

16. Orazem, Mark E., and John Newman, "Primary Current Distribution and Resistance of a Slotted–Electrode Cell," *Journal of the Electrochemical Society* **131** (1984), 2857–2861.

17. Orazem, Mark E., "Calculation of the Electrical Resistance of a Compact Tension Specimen for Crack–Propagation Measurements," *Journal of the Electrochemical Society* **132** (1985), 2071–2076.

18. Brown, Robert A., L. E. Scriven, and William J. Silliman, "Computer–Aided Analysis of Nonlinear Problems in Transport Phenomena,"in *New Approaches to Nonlinear Problems in Dynamics*, P. J. Holmes, editor, Soc. Ind. Appl. Math., Philadelphia, 1980, 289–307.

19. Milne–Thomson, L. M., "Jacobian Elliptic Functions and Theta Functions" and "Elliptic Integrals," chapters 16 and 17 in *Handbook of Mathematical Functions*, edited by M. Abromowitz and I. A. Stegun, Dover Publications, New York, 1972.

DISTRIBUTION LIST

Copy No.	
1	Office of Naval Research 800 N. Quincy Street Arlington, VA 22217-5000 Attention: Dr. A. John Sedriks Materials Division, Code 1131M
2 - 7	Director Naval Research Laboratory Washington, DC 20375 Attention: Code 2627
8 - 19	Defense Technical Information Center, S47031 Building 5, Cameron Station Alexandria, VA 22314
20 - 21	Dr. M. E. Orazem, CHE
22	Dr. E. L. Gaden, Jr., CHE
23 - 24	Ms. E. H. Pancake, Clark Hall
25	SEAS Publications Files
*	Office of Naval Research Resident Representative 818 Connecticut Avenue, N.W. Eighth Floor Washington, DC 20006 Attention: Mr. Michael McCracken Administrative Contracting Officer

*Send cover letter only

1618:ald:DW212R

UNIVERSITY OF VIRGINIA

School of Engineering and Applied Science

The University of Virginia's School of Engineering and Applied Science has an undergraduate enrollment of approximately 1,500 students with a graduate enrollment of approximately 560. There are 150 faculty members, a majority of whom conduct research in addition to teaching.

Research is a vital part of the educational program and interests parallel academic specialties. These range from the classical engineering disciplines of Chemical, Civil, Electrical, and Mechanical and Aerospace to newer, more specialized fields of Biomedical Engineering, Systems Engineering, Materials Science, Nuclear Engineering and Engineering Physics, Applied Mathematics and Computer Science. Within these disciplines there are well equipped laboratories for conducting highly specialized research. All departments offer the doctorate; Biomedical and Materials Science grant only graduate degrees. In addition, courses in the humanities are offered within the School.

The University of Virginia (which includes approximately 2,000 faculty and a total of full-time student enrollment of about 16,400), also offers professional degrees under the schools of Architecture, Law, Medicine, Nursing, Commerce, Business Administration, and Education. In addition, the College of Arts and Sciences houses departments of Mathematics, Physics, Chemistry and others relevant to the engineering research program. The School of Engineering and Applied Science is an integral part of this University community which provides opportunities for interdisciplinary work in pursuit of the basic goals of education, research, and public service.